National Library of Canada
Acquisitions and Bibliographic Services Branch
395 Wellington Street
Ottawa, Ontario
K1A 0N4

Bibliothèque nationale du Canada
Direction des acquisitions et des services bibliographiques
395, rue Wellington
Ottawa (Ontario)
K1A 0N4

Your file Votre référence

Our file Notre référence

NOTICE

The quality of this microform is heavily dependent upon the quality of the original thesis submitted for microfilming. Every effort has been made to ensure the highest quality of reproduction possible.

If pages are missing, contact the university which granted the degree.

Some pages may have indistinct print especially if the original pages were typed with a poor typewriter ribbon or if the university sent us an inferior photocopy.

AVIS

La qualité de cette microforme dépend grandement de la qualité de la thèse soumise au microfilmage. Nous avons tout fait pour assurer une qualité supérieure de reproduction.

S'il manque des pages, veuillez communiquer avec l'université qui a conféré le grade.

La qualité d'impression de certaines pages peut laisser à désirer, surtout si les pages originales ont été dactylographiées à l'aide d'un ruban usé ou si l'université nous a fait parvenir une photocopie de qualité inférieure.

Canada

EXPERIMENTAL STUDIES ON FLOW AND NOISE GENERATED FROM SINGLE AND TWIN SUPERSONIC UNDEREXPANDED JETS

Alireza Roshanzamir

A Thesis

in The Department of Mechanical Engineering

Presented in Partial Fulfilment of the Requirements

for the

Degree of Master of Applied Science

at

Concordia University

Montreal, Quebec, Canada

May, 1994

ISBN 0-315-97632-2

Canada

ABSTRACT

Experimental Studies on Flow and Noise Generated From Single and Twin Supersonic Underexpanded Jets

Alireza Roshanzamir

The flow and noise generated from single and twin supersonic jets were studied experimentally for a wide range of jet pressure ratios. Optical and acoustical data were obtained. A single, and three twin chocked tube models were used to generate supersonic underexpanded jets.The centre-to-centre spacings of twin jets were chosen 1.6, 1.8, and 2.0 times of internal tube diameter. Spark schlieren photography was employed to determine the change in the jet structure and shock cell length. It was found that the average shock cell of twin-jet is longer than that of single jet. Acoustical data were obtained by placing a microphone in the exit plane of tube which was connected to a signal analyzer. The screech tone frequency and amplitude were measured for single and twin jets by using these data. The decrease of the screech tone frequency with increasing pressure ratio was interrupted by three frequency jumps. Effect of different configurations and centre-to-centre spacings on screech tones were achieved. It was found that the twin-jet screech tone frequency was lower than that of single jet at a given pressure ratio. However, the twin-jet screech tone amplitude is higher than that of single jet. From

optical and acoustical results two relations were obtained to determine the average shock cell length and screech frequency for twin-jet.Twin-jet screech tone amplitude was found to exceed the sonic fatigue level reference of aircraft metallic structure. In order to suppress the high amplitude, small rectangular tabs were placed at the exit plane of the tube. These tabs reduced screech tone amplitude to below the sonic fatigue level.

ACKNOWLEDGMENTS

The author would like to express his gratitude to his supervisor Dr. R. A. Neemeh for his continued guidance, encouragement, advice, and constructive criticism throughout the course of this study.

Special thanks are due to his wife for her understanding and support during the course of this investigation.

TABLE OF CONTENTS

LIST OF FIGURES

NOMENCLATURE

a_o	Ambient Sound Speed
a_j	Jet Sound Speed
c	Speed of Light in Vacuum
c_o	Speed of Light in Medium
D	Nozzle Exit Diameter
D_j	Fully Expanded Jet Diameter
f_s	Screech Tone Frequency
L	Average Shock Cell Length
M	Mach Number
M_c	Convection Mach Number
M_d	Design Mach Number
M_f	Forward Flight Mach Number
M_j	Fully Expanded Jet Mach Number
n	Index of Light Refraction
NPR	Nozzle Pressure Ratio
p	Root Mean Square of Sound Pressure
p_o	Reference Sound Pressure (20 μPa)
P_a	Ambient Pressure
P_b	Back Pressure

P_e Exit Static Pressure

P_c Chamber Pressure

S Centre-to-Centre Nozzle Spacing

SPL Sound Pressure Level (re 20μPa)

St Strouhal Number

t Time

T_a Ambient Temperature

T_j Jet Temperature

T_o Total Pressure

T_r Reservoir Temperature

v Piston Velocity

V_c Convection Velocity

V_j Fully Expanded Jet Velocity

x X-Coordinate

y Y-Coordinate

α Angle of Light Deflection

β $(M_j^2-1)^{1/2}$

γ Ratio of Specific Heats

λ Acoustic Wavelength

ρ Density

CHAPTER 1

INTRODUCTION

Advanced jet engine designs for supersonic and subsonic aircrafts can be operated at off design conditions. The noise produced due to the presence of shock waves in a supersonic jet has a direct application to the future design of commercial supersonic aircraft exhaust nozzles and is an important factor in community noise and structural fatigue.

Aerodynamic noise due to supersonic jets consists of two principal components, namely, *turbulent mixing and shock noise*. Turbulent mixing noise is the dominant noise in shock free jets. It is proposed [1][1] that this kind of noise is generated by interaction of the large scale turbulence structure with ambient air. The large scale turbulence structure not only generate the dominant part of the noise in shock free supersonic jets, but is also responsible for producing shock noise, when the supersonic nozzle is operated using off-design conditions. When a nozzle is operated at a nozzle pressure ratio, P_r / P_b , greater than the design value, a periodic shock cell system occur in the exhaust plume. The shock cell structure of an imperfectly expanded supersonic jet is formed by oblique shocks and expansion fans generated at the lip region where there is mismatch of the static pressure inside and outside the jet. Oblique shocks and expansion fans impinge on

[1]The number within brackets represents the number of reference.

the jet boundary and are reflected back into jet resulting in periodic shock cells. The strength of the shocks depends on the nozzle design condition on which the nozzle is operated. As the large scale turbulence structures propagate down stream, they interact with the periodic shock cell in the imperfectly expanded jet and generate another noise called shock noise.

Supersonic jet shock noise contains two components. The first, a high-amplitude discrete tone, called *screech tone*, which was first studied by Powell [2]. He investigated optically the flow and the adjacent acoustic fields. Based on the results of his observations he concluded that the screech tones were generated by feedback loops. According to Powell, the feedback loop of each tone consists of downstream propagating flow disturbances created at the nozzle lip region. As these disturbances passed through the third or fourth shock cell, strong interactions with the oblique shocks took place resulting in emission of intense acoustic waves. Part of the acoustic waves propagated upstream outside the jet flow. Upon reaching the nozzle lip these acoustic waves triggered the generation of downstream propagating flow disturbances and thus completed the feedback loop. Harper-Bourne and Fisher [3] were the first to investigate the second component of shock noise, *broadband shock noise,* in detail and suggested a mechanism based on an extension of Powell's screech model. This broadband shock associated noise is in general easily distinguishable from the turbulent mixing noise.

When two supersonic jets are closely spaced, the level of the screech tone

can be greatly amplified due to a coupling process between the two jets [4]. This high amplitude-narrow band tone can exceed the fatigue sonic level of aircraft structure. Aircrafts such as F-15 and B-1B use a very closely spaced engine configuration, and each is known to have suffered fatigue failures to engine nozzle outer flaps in the internozzle region [5,6]. Although the screech tone from single jets has been extensively studied, the screech tone for two closely spaced jets has only been investigated by a few researchers. References [4-9] represent most of the works that have been directed toward the twin-jet screech problem.

The objective of this study was therefore to obtain additional optical and acoustic information on supersonic jet screech tone in single and twin jets. Schlieren photography was employed for flow visualization and shock cell length measurements. Acoustic measurements were carried out to determine the screech tone characteristics and the effect of small rectangular tabs, placed at the exit plane of the nozzle, on noise suppression.

In chapters 2 and 3, some concepts and definitions of jet aerodynamics and shock noise mechanism generation will be first introduced. The experimental setup, and results will be followed by conclusions and future recommendations, presented in chapter 6.

CHAPTER 2

CONCEPTS AND DEFINITIONS

In this chapter some concepts and definitions that are related to this study will be explained.

2.1 Wave Motion

The changes that may occur at a given point in a medium are communicated to other points through wave motions. There are four types:

(a) Infinitesimal pressure waves (sound waves)

(b) Non-steep pressure waves with finite amplitude

(c) Steep pressure wave (shock wave)

(d) Expansion waves

2.1.1 Propagation of infinitesimal waves (sound wave)

Sound waves are defined as infinitesimal pressure waves. The changes across such a wave are small and the speed of the process corresponding to these changes is fast. Therefore, neglecting heat transfer, the changes across an infinitesimal pressure wave can be assumed adiabatic and reversible or isentropic. Figure 2.1 shows the propagation of an infinitesimal pressure wave into a stagnant gas. Such a wave is generated by the sudden movement of a piston in a cylinder with an infinitesimal velocity dv. The wave propagates to the right with sound

velocity a into the stagnant gas which was initially maintained at a pressure P_1 and a temperature T_1 . After the passage of the wave, the pressure and temperature of the gas increase to $P_1 + dP$ and $T_1 + dT$, respectively.

2.1.2 Non-Steep Finite Pressure Waves

If the impulses are continuously generated by the piston through its gradual acceleration, finite changes in the pressure and other quantities will occur. As shown in figure 2.2 these changes are made up of a number of infinitesimal isentropic ones that make the overall change across the wave continuous (non-steep) and isentropic. The waves propagate to the right into the stagnant gas (pressure P_1 and temperature T_1) and set it into motion with a velocity v and pressure P. The space-time diagram for the system of waves along with the trajectory of the piston and space-pressure diagram are shown in figure 2.2. The pressure, temperature and sound velocity increase isentropically to higher values. The particle velocity also increases progressively which makes the waves generated in the later stages propagates at higher absolute velocities than the preceding ones. This fact is demonstrated by the decreasing slope of the subsequent waves on the time-space diagram.

2.1.3 Steep Finite Pressure Waves

As the pressure waves generated by the impulsive motion of the piston in the preceding case propagates downstream, the faster moving waves tend to overtake the slower ones generated earlier. Figure 2.3 shows a condition when a

number of compression waves merge into one *finite steep pressure wave or shock wave*. Unlike the infinitesimal and non-steep finite compression waves the changes across the steep wave are not reversible and therefore not isentropic.

2.1.4 Expansion Waves

An expansion wave is one which reduces the pressure of the fluid through which it is propagating. A sudden outward motion of the piston in a cylinder generates an expansion waves. An infinitesimal expansion wave is shown in figure 2.4. This wave is moving towards the right at the velocity of sound into the stagnant gas having a pressure and temperature of P_1 and T_1, respectively. The wave reduces the pressure and temperature of the gas and makes it move to the left with the piston velocity *dv*.

2.2 Formation of The Large Scale Structure

The following four flow regimes can be distinguished during the development of the large scale structures [10].

- Instability: the shear layer produced by the lip wake and nozzle boundary layer is intrinsically unstable (whether turbulent or not) and develops periodic oscillations.

- Vorticity concentration: as the amplitude of the oscillations, increases the vorticity tends to be concentrated in separated region.

- Formation of vortex-ring-like structure: the concentrated regions of vorticity

clearly display their ring-like structure as their scales approach the jet diameter.

- Vortex interaction: neighbouring vortex-rings interact with each other in the following manner, one decelerates and the other accelerates, until the two pair with each other, doubling the size of both the vorticity concentration region and the spacing between adjacent vorticity concentration. The rate of pairing determines the spreading rate of the layer and, thus, the length of the potential core. The pairing process is believed to be the key to understanding the turbulent mixing process as well as the noise generation.

2.3 Aerodynamic of Shock Containing Supersonic Plumes

The purpose of this section is to exhibit certain aerodynamic characteristics of shock containing supersonic jet plume that have a rational association to the physical mechanism of shock noise.

2.3.1 Isentropic Flow in a Converging Nozzle

Figure 2.7 shows the pressure distribution obtained in the nozzle for six different values of back pressure. For curve 1, there is no flow in the nozzle, and pressure is invariant with x. As the back pressure decreases below the tank pressure, P_r , more and more flow is induced though the nozzle (curves 2 and 3). The static pressure decreases with x and the velocity at the nozzle exit plane increases until it eventually reaches the sonic value (curve 4). If the back pressure decreases below the value corresponding to sonic conditions, the flow

characteristics inside the nozzle remains the same. The flow adjusts to the new back pressure outside the nozzle by means of Prandtl-Meyer expansion fans as shown in the figure [11]. The flow in the nozzle under these conditions is said to be chocked (curve 4). Here, the pressure ratio, P_b / P_r can be calculated for isentropic flow through the nozzle. For a perfect gas with constant specific heats,

$$P_t = P_b(1+\frac{\gamma-1}{2}M^2)^{\gamma/(\gamma-1)} \tag{2.1}$$

For isentropic flow in the nozzle, P_t is constant and equal to the tank pressure, P_r , and the Mach number is equal to unity, therefore,

$$\frac{P_r}{P_b} = (\frac{\gamma+1}{2})^{\gamma/(\gamma-1)} \tag{2.2}$$

for air γ = 1.4 and P_b / P_r = 0.5283. This ratio is termed as the critical pressure ratio below which the nozzle is chocked.

2.3.2 Exit Flow of Supersonic Nozzle

When the back pressure is below the critical value, the flow expansion inside the nozzle is insufficient to reach the back pressure at the nozzle exit plane and Prandtl-Meyer expansion fans form as shown in figure 2.8. The pressure across the expansion fans (region 2) reduces to the back pressure value. Here the flow expansion is similar to that around a convex corner which involves smooth and gradual change in flow properties [11]. For this isentropic process, with no change

in stagnation pressure, the Mach number in region 2 can be determined from the following relation:

$$M_2 = [[(\frac{P_t}{P_b})^{\frac{\gamma-1}{\gamma}} - 1]\frac{2}{\gamma-1}]^{\frac{1}{2}} \tag{2.3}$$

Note that M_2 is also defined as the jet Mach number M_j. The jet velocity V_j is defined as:

$$V_j = M_j a_j \tag{2.4}$$

where a_j is the jet sound velocity calculated at the jet temperature T_j which in turn is a function of the total temperature T_t.

$$T_j = \frac{T_t}{1+\frac{\gamma-1}{2}M_j^2} \tag{2.5}$$

The expansion waves at the nozzle exit reflect from the jet boundary as compression waves which merge together to form the oblique shock with pressure in region 5 higher than the ambient pressure. The oblique shock reflects from the jet boundary as centred expansion waves and the cyclic process repeats. This flow pattern appears as a series of shock cells.

2.3.3 Description of General Plume Features

Figure 2.9 illustrates, as an example, the underexpanded flow produced by a supersonic nozzle [13]. The inner edge of the mixing layer is outlined by the

inter cone whose axial extent defines the length of the initial mixing layer. The outer solid lines in figure 2.9 show the radial extent of the outer edge of the mixing layer which, along with the lower edge of the mixing layer, characterizes the rate of plume spreading. The region of supersonic flow is enveloped by the sonic line, shown here by the dashed cone. It represents the boundary for shock wave terminations.

It is evident that the repetitive shock wave pattern, which forms the diamond - shape cell in schlieren photograph extends well beyond the nozzle exit, providing a large area for shock - turbulence interaction. The shocks located near the end and beyond the initial mixing region are referred to as downstream shocks. All shocks in the turbulent mixing zone are curved since they propagate into a region of nonuniform mean flow. This curvature is responsible for the gradual steeping of the wave angle relative to the mean flow which leads to an observable decrease in shock cell spacing with axial distance. Eventually a point is reached where the shock can properly adjust the flow and the wave is cancelled. This occurs before the end of the supersonic core [13].

Having completed the consideration of basic aerodynamic concepts of the supersonic jet, the mechanism of shock noise generation will be discussed.

CHAPTER 3

MECHANISM OF SHOCK NOISE GENERATION

In an improperly expanded supersonic jet, the static pressure of the flow at the nozzle exit differs from the ambient pressure. This pressure difference causes a shock system to form in the jet exhaust plume. Along the boundary of the jet, a turbulent shear layer develops and generates the turbulent mixing noise. A sonic line for the flow velocity profile is located within the shear layer, and the embedded shock system in the jet plume will not extend beyond this line. The segment of the shock located in the mixing layer zone is considered a source of acoustic radiation due to shock vortex interaction [14]. A typical configuration of a shock containing supersonic jet is shown in figure 3.1.

3.1 The Dynamics of Shock Noise Generation

Figure 3.2 shows the interferograms from the experimental shock vortex interaction [15]. The evaluation of the interferograms gives the time dependent density fields. In figure 3.2a the interacting shock wave reaches the test region from the right. As the shock propagates towards the vortex centre it becomes curved. Beyond the vortex centre, a discontinuity on the shock front occurs and a weak secondary wave (sound wave) is formed. Typical computed results of shock-vortex interaction are shown in figure 3.3 [14]. A clockwise-rotating vortex

embedded in the supersonic freestream is convected through a shock front from left to right. The interaction between the shock and the vortex creates a complex pressure pattern behind the shock. In figure 3.3 , the pressure contours are normalized with respect to the unperturbed pressure downstream of the shock. The centre of the vortex is shown as a deep pressure depression with its centre marked with a cross. The region above the vortex centre is at a higher pressure than the steady-state condition whereas the region below the vortex centre is at a lower pressure than the steady-state condition. The regions of high and low pressure are marked by H and L, respectively. The location of the acoustic wave front is indicated by a circle with dash lines.

It should be noted that the region of high pressure is developed at the point on the shock where the velocity induced by the vortex forces the shock to deflect downstream, thereby compressing the downstream flow. Similarly, the region of low pressure is developed at the point on the shock where the vortex pulls the shock upstream, thereby expanding the downstream flow. In order to verify the acoustic nature of the wavefront, a plot of wavefront radial distance from the vortex centre against the time elapsed since the vortex centre passed over the shock was used . The wavefront was noted to move linearly with time. The slope of this line gives the speed of propagation of the wave front, which in this case is found to be equal to the local speed of sound.

The kinematics of a vortex interacting with a normal shock can be

transposed to the situation in which the vortex interacts with an oblique shock [14]. A sketch is shown in figure 3.4 of the typical geometry of shock vortex interaction in a jet. A vortex convected at supersonic speed is shown passing through the downstream facing conical segment of the shock, the vortex continues to move downstream at a lower supersonic speed. The radiated acoustic wave front is expanded and convected in a direction parallel to the shock front. The segments of the acoustic wave front with the highest intensity move outward along the shock, into the subsonic portion of the shear layer, and finally into the far field. The interaction between a vortex and the upstream facing conical segment of the shock surface can also generate noise.

Both experimental [15] and numerical [14,16] results clearly show that sound is produced when a fluid disturbance, in this case a vortex, is moving at a relative speed to a shock and interacts with the shock wave.

The upstream noise radiation from a shock containing a supersonic jet is dominated by a *broadband shock associated noise* along with one (or more) high amplitude tones known as *jet screech tone*. Powell [2] developed a model to predict the discrete component, and later Harper-Bourne and Fisher [3] developed a model to predict the broadband shock noise component.

3.2 Broadband Shock Associated Noise

Tam and Tanna [17] investigated both theoretically and experimentally the

broadband component shock. They proposed that broadband shock associated noise is generated by the weak interaction between downstream propagation of large turbulence structures and quasi-periodic shock cell structures of the jet. Tam, Seiner and Yu [18] proposed that screech could be considered as a very special case of broadband shock associated noise.

3.3 Screech Tone

High-amplitude discrete tones, called screech, were first studied by Powell [3]. Powell's explanation of the screech process involves a feed back loop consisting of flow disturbances and sound waves. The disturbances are formed at the nozzle lip and travel downstream to interact with the shock structure. This interaction produces noise which travels upstream and creates additional disturbances upon passing the nozzle. This process led to an acoustic model where stationary sources were located at the ends of the shock cells, with phasing between them determined by the convection velocity of the disturbance. He noted that increases in nozzle pressure ratio were accompanied by an increase in screech tone wavelengths, and that the tone had a tendency to propagate back to the nozzle exit. The screech data of Powell's consisted of discontinuous and disjoint frequency.

3.3.1 Screech Tone Frequency

The formula derived from Powell's model can be written for the fundamental screech frequency as

$$f_s = \frac{V_c}{L(1+M_c)} \tag{3.1}$$

where L , V_c , M_c are the distance between the monopole source, convection velocity, and Mach number of turbulent eddies, respectively [19]. Using the crossed laser beam experiments of Harper- Bourne and Fisher [3], the convection velocity of the large scale structure is estimated as,

$$V_c = 0.7V_j \tag{3.2}$$

The convection Mach number M_c is related to convection velocity by,

$$M_c = \frac{V_c}{a_o} \tag{3.3}$$

where a_o is ambient sound velocity. The screech frequency f_s can be written in terms of a nondimensional Strouhal number as,

$$St = \frac{f_s D_j}{V_j} = \frac{V_c(D_j/D)}{V_j(L/D)(1+M_c)} = \frac{0.7(D_j/D)}{(L/D)(1+M_c)} \tag{3.4}$$

and from Tam and Tanna [17] the ratio of the fully expanded jet diameter D_j to the jet exit diameter D is given by,

$$\frac{D_j}{D} = \left[\frac{[1+(\gamma-1)/2]M_j^2}{[1+(\gamma-1)/2]M_d^2}\right]^{(\gamma+1)/4(\gamma-1)} \left(\frac{M_d}{M_j}\right)^{1/2} \tag{3.5}$$

where M_j and M_d are jet Mach number and design Mach number, respectively. In equation 3.4, the distance between the monopole source is approximated by the average shock cell length L.

3.3.2 Influence of Temperature and Forward Flight on Jet Screech

For many years it was thought that jet screech phenomenon would not be present in full scale engines due to irregular nozzle exit conditions, non-uniform exit velocity profiles and jet exhausts [19]. Roshford and Tam [20] investigated the effect of the jet total temperature T_o on jet screech from a sonic nozzle with M_j and T_o ranging respectively to 1.9 and 800 °K. They showed that with increased heating the screech frequency increases for a fixed value of M_j .

The influence of flight on noise emitted by jet flows is extremely important in assessing whether one would expect sonic fatigue to occur. In supersonic flight, the noise generated by interaction of disturbances with shock waves is not considered to play a fundamental role, since one expects to see partial transmission of plume shocks to free space. However, even for current generation supersonic fighter aircrafts, the majority of flight hours involve operation at subsonic forward flight speeds where the nozzle pressure ratio is still supercritical. The study of shock generated noise with simulated forward flight represents a reasonably new

area for current research [21-24], and one which requires much more research to derive full understanding of the physical process involved. Norm and Shearin [24] investigated the behaviour of the unheated sonic plume with relatively low forward flight speed (i.e., $M_f = 0.15$). Their static pressure data shows that with an increase in flight speed there is a slight increase in downstream shock cell length and the screech frequency in flight is reduced, as might be expected from equation 3.1 due to a slight increase in L. This illustrates that the preferred model structure of jet screech can be strongly influenced by forward flight.

3.3.3 Location of Principle Region For Jet Screech Emission

From the theoretical work of Tam and Burton [25] and Morris and Tam [26] and the experimental work of McLauhlin, Morris, and Troutt [27] the most unstable shear layer modes grow rapidly in the annular region of flow, achieve neutral stability near or slightly beyond the jet potential core, and decay beyond this region. These findings provide a plausible explanation for the observation that screech is principally generated from regions typically beyond the third shock cell [19].

3.3.4 Influence of Nozzle Lip Thickness

The influence of the reflecting surface of the nozzle lip thickness was realized in the early investigations by Powell [2]. Large reduction of screech amplitude (about 10 dB) was obtained by the experiments of Nourm [28], when the lip thickness was eliminated. Thus the geometric detail is an important one

where screech tone are concerned.

3.4 Twin-jet Screech Tone

Single jet noise has been extensively studied whereas the noise and coupling process between two closely spaced jets have only been investigated recently by a few researchers. The amount of research directed towards reducing twin-jet screech amplitude is even more limited.

Berndt's dynamic pressure measurements [7]on the B-1A aircraft suggest that damage could be related to the existence of a high-energy narrow-band process in the internozzle region. T. G. Norum and J. G. Shearint [5] used a small model B-1 aircraft, and found that closely spaced twin-jets oscillate to a much greater extent than a corresponding single jet over a wide range of nozzle pressure ratios. The twin-jet acoustic level that propagates upstream to the exhaust nozzles can be exceed the single jet level by more than 20 dB. It is suggested the structural damage found in supersonic twin-jet configurations may be caused by that acoustic resonance.

Seiner et al [6] carried out a series of noise and optical measurements on a 1/40-th scale twin supersonic jet with powered chocked axisymmetric nozzles. The mechanism of twin supersonic jet resonance and its properties as a possible mechanism of engine flap fatigue failure on the F-15 and B-1B aircraft was studied. It was found that excessive internozzle dynamic pressures exceed the sonic

fatigue failures of metallic aircraft structure. Suppression concept investigated in their study involved minor geometric change to the nozzle.

The role of jet spacing in dynamic plume interaction was studied by R. W. Wlezien [8]. The normalized centre to centre spacing, *S/D*, of the nozzles was carried over the range $1.8 < S/D < 3.2$. It was found when spacing is small the plumes merged before the higher modes developed and screech was thereby suppressed. For greater spacings, the dominant modes developed farther downstream where the shear layer was large.

3.5 Suppression of Screech Tone Amplitude

Methods used to suppress chocked jet noise were investigated in the early fifties by Powell. He clearly showed that thickening of the shear layer at the jet exit would reduce the generated noise. He used notches and radial vanes to thicken the shear layer. Bradbury and Khadem [29] conducted a study on the jet under the influence of tabs. They used rectangular tabs in a subsonic jet and observed a significant increase in the jet centreline velocity decay when two tabs were located 180 deg apart at the nozzle exit. The effect of varying exit geometry was investigated by Norum [28]. The amplitude was reduced by about 10 dB when the lip thickness was eliminated, and another 10 dB when the periphery was disrupted. Small modifications to the external surface of the tube at the jet exit was noted to have a large effect on the amplitude of the screech process. Samimy [30] studied

the effect of tabs on the flow and noise field of an axisymmetric jet. The tabs were found to weaken the shock structure drastically in the supersonic regime which was accompanied by an elimination of the screech noise.

The amount of research directed toward reducing twin-jet screech amplitudes is limited. However, the work for screech suppression of single jets can be applicable to twin-jet because if one jet is suppressed, the two jets are decoupled, and the screech amplitude is reduced [4]. Shaw [4] found small tabs located at the exit plane to be very effective suppressor if they were large enough or if multiple tabs were installed.

CHAPTER 4

EXPERIMENTAL SETUP

The experiments were conducted in the shock-wave dynamics research laboratory.

4.1.1 Experimental Apparatus

Three chocked-tube nozzles were employed. They were 57 *mm* long and had an internal diameter of 12 *mm*. The centre-to-centre line spacings were chosen at 1.6, 1.8, and 2.0 times the internal nozzle diameter. The twin nozzles were fixed to an aluminum plate which was mounted to a large cylindrical plenum chamber. Figure 4.1 shows a sectional view of the twin-chocked model. The pressure in the chamber was measured by means of a pressure gauge mounted as shown in figure 4.2. The chamber was supplied by air from a large high pressure tank.

4.1.2 Schlieren System (Optical Setup)

Top view of the schlieren system is shown in figure 4.3. A 4KV spark light source was employed, connected to a flash power supply, which supplies a light pulse of a few microsecond for instantaneous photography of the flow. An air-cooled concentrated Arc lamp connected to a power supply unit was used for video records. The light source was located in front of condenser lenses 1 and 2. These lenses were used to obtain an effective light source, and focus the light rays on the

knife edge. The knife edge was made of four razor, set on an adjustable frame. The knife edge had to be positioned at the focal point of a parabolic mirror to yield parallel light beams passing through the test section and reflecting on another parabolic mirror. The two parabolic mirrors were 15 *cm* in diameter and had a focal length of 122 *cm*. The second mirror converged the light rays to the focal point where another knife edge was used. The knife edge was a razor blade held in position by a frame on a stand. It cut some part of the light, producing the schlieren effect, in such a way that only a certain fraction (often about half) of the light enters the camera. The knife edge was oriented vertically so that density gradients in the flow were along the axis of jet.

A polaroid land camera, without lens, was used to take instantaneous photographs. A Sony Hi-88 was employed for video recording. The camera was placed on an adjustable stand. The fundamental concepts of the optical measurement is described in Appendix A.

4.1.3 Acoustic Setup

For noise measurements, a *B&K* 4181 microphone was used to convert the pressure signal to an electrical signal. Before each run the microphone was calibrated with a *B&K* calibrator. The signals from the microphone were routed to a signal analyzer type 2035 to display the *SPL* levels during the test. The signal analyzer unit, type 2035, is a mainframe unit fitted with a 12" raster scan screen, a disk drive and a keyboard. It houses the signal and display processors, the

memories, and all the hardware that is needed for analysis and system control [31]. Having measured the signals, the data may be converted to the *ASCII* mode, and stored on 3.5" disks for later analysis using a P.C. Freelance software was employed to plot the spectra. Figure 4.4 shows the experimental setup for noise measurements.

4.2 Procedure

Two separate runs were made with each model to obtain the acoustic and optical information. The jet pressure ratio was adjusted and maintain constant for the duration of the run. The chamber pressure was recorded after the jet flow had attained equilibrium. Using isentropic relationships, the jet Mach number for each test can be determined,

$$M_J = \left[\frac{2}{\gamma - 1}\left[\left(\frac{P_c}{P_a}\right)^{\frac{\gamma-1}{\gamma}} - 1\right]\right]^{1/2} \tag{4.1}$$

where: P_c is chamber pressure.

P_a is ambient pressure.

4.2.1 Optical Procedure

Before taking the photographs, the lenses and mirrors were cleaned. The lens were located at a certain distance from the light source and mirror to provide the required light intensity. The angle between the light source and the mirror axis was ensured not to be more than 10° [32]. The position of the knife edge was carefully

chosen to yield required picture contrast. After adjusting the flow and turing all light off, the diaphragm of camera was opened and the flow was exposed to the spark light for a few microseconds.

4.2.2 Acoustical Procedure

After the jet flow was established the calibrated microphone was held at the exit plane of the nozzle for a few seconds. The position of the microphone is shown in figure 4.4. The frequency domain can be seen directly on the signal analyzer screen. The data may be stored on a disk for later analysis. Acoustic spectra were obtained for 28 nozzle pressure ratios ranging from 2.22 to 4.06 for single and twin nozzles, and 7 nozzle pressure ratios for twin jets (S/D=2.0) with tabs. These data set included 140 spectra, each with frequency varying from 0 to 25 KHz.

Measurements of sound pressures required special attention. The microphone was placed away from other vibrating components (i.e. nozzle) to avoid additional signals appearing in the microphone output. Single jet data were obtained by blocking off the flow through one the tubes.

CHAPTER 5

RESULTS AND DISCUSSION

In this chapter optical and acoustical results of single and twin jets will be presented. These results were expressed in the form of either semi-empirical formulas or graphical charts so that they may be utilized generally. Figure 5.1 shows the experimental process used to obtained these results.

5.1 Optical Measurement Results

Optical results were obtained by employing the schlieren system which was described earlier. Both spark and continuous light sources were used. Schlieren photographs with an exposure of a few microseconds were taken to display the jet structure.

5.1.1 Flow Visualization

The variation in the structure corresponding to the different jet Mach numbers is visualized using spark schlieren photography. The shock cell structures consist of a series of oblique shocks and expansion fans impinging on, and reflecting from the jet boundaries. Figure 5.2 shows the third shock cells are displaced outward from the plane of symmetry between the plumes, and the fourth cells are displaced inward. A comparison between the top view and the side view shows the helical mode. The optical results also demonstrated that shock cell

length, for both single and twin-jet configurations, increased with increase in pressure ratio, and corresponding jet Mach number. Figure 5.3 shows typical photographs of variation in shock cell length for twin-jet configuration (*S/D*= 1.8). The effect of different configurations on shock cell structures can be seen in figure 5.4. It was found that the twin-jet average shock cell length is slightly longer than that of single jet. This difference may be due to the turbulent mixing layer and the coupling process between the two jets. The effect of centre-to-centre spacings on shock cell length of twin-jet configurations can be seen in figure 5.5. At a given jet Mach number, the shock cell lengths for the three models are almost equal. Therefore the twin-jet shock cell length is almost independent of centre-to-centre spacing.

5.1.2 Average Shock Cell Length

It is of interest to determine the variation of shock cell length with jet Mach number, in order to predict screech tone frequency. The average shock cell lengths were measured for 13 pressure ratios, corresponding to jet Mach numbers of 1.18 to 1.56. The average shock cell length, *L*, was normalized by jet exhaust diameter *D*. Figure 5.6a shows the results of the average shock cell lengths as a function of β for single jet. Based on the results the relation given below can be obtained

$$\frac{L}{D} = 1.13\beta^{1.29} \qquad (5.1)$$

In figure 5.6a the dashed curve was plotted using equations 5.2 [12].

$$\frac{L}{D} = 1.16\beta \tag{5.2}$$

Similar tests were carried out for twin-jet configurations. As previously noted the different centre-to-centre spacings had no significant effect on shock cell lengths of twin-jet. The results are presented in figure 5.6b. Based on these results, the following equation was obtained to determined twin-jet average shock cell length

$$\frac{L}{D} = 1.17\beta^{1.36} \tag{5.3}$$

5.2 Acoustic Measurement Results

Acoustic spectra were obtained for 28 pressure ratios between 2.224 and 4.061, corresponding to fully expanded jet Mach numbers M_j between 1.133 and 1.569, for single and twin tube configurations at three different spacing, S/D=1.6, 1.8 and 2.0. These data set included 112 spectra, each with frequency from 0 to 25 KHz.

5.2.1 Single Jet Results

Figure 5.7 shows two typical noise spectra. These particular spectra were obtained by operating the single chocked tube at jet Mach numbers 1.133 and 1.534 .

The spectra consist of the different noise generation mechanisms, namely the

turbulent mixing noise and the shock noise. At very low jet Mach number, M_j = 1.133, the supersonic jet almost ideally expanded and the turbulent mixing noise is the dominant component. This kind of noise is generated by the interaction of the large scale turbulent structure in the jet flow and the ambient fluid.

At off-design condition, M_j =1.534, when the large turbulent structure interacts with the shock cell in the imperfectly expanded jet the shock noise is generated as well. The shock noise mechanism produces the discrete screech component and the broadband shock noise. Figure 5.7 shows that the broadband component dominates the turbulent mixing noise . The high amplitude screech tone and its first harmonic can clearly be observed at about 11 KHz and 22 KHz. respectively. The study of this high amplitude tone is the main subject of the acoustics measurement.

a) Identification of Modes

Previous studies of screech tone [33,34] indicated that it consisted of several stages depending on nozzle pressure ratio. Powell noted that increase in nozzle pressure ratios was accompanied by decrease in screech tone frequency. The screech data of Powell's consisted of discontinuous and disjoint frequency jumps with pressure ratio for axisymmetric jets. The screech tone data presented in figure 5.8 is included to illustrate what have been typically observed by other researchers.

At very low jet Mach number (figure 5.8a) no discrete tone can be observed over the range of study. By increasing the pressure ratio corresponding to M_j

=1.262, the stage *A* (toroidal mode) of the screech at 17 KHz, and the stage *B* (helical mode) at 12.5 KHz can be seen. Figure 5.8c shows the noise spectra at M_j =1.317. Frequencies of both stages are decreased by increasing the pressure ratio, however stage *B* is dominant. At middle jet Mach number M_j =1.383, the stage *C* appeared at 12.5 KHz. In this particular case, three stages of screech tone can be observed simultaneously, however stage *B* still dominant. Figure 5.8e shows that at higher jet Mach number the stage *A* completely vanishes and two other stages are present. Finally at high jet Mach number, M_j=1.546, the stage *C* is dominant and stage *B* almost disappears.

b) Screech Tone Frequency

The frequency of screech tone f_s from equation (3.1) (nondimensionalized by D_j / V_j) can be written in term of the Strouhal number as,

$$St = \frac{f_s D_j}{V_j} = \frac{0.7(D_j/D)}{L/D(1+M_c)} \tag{5.4}$$

Substituting the average shock length equation 5.1 from optical results, the following relation can be obtained

$$St = \frac{0.7(D_j/D)}{1.13(M_j^2-1)^{1.29}(1+M_c)} \tag{5.5}$$

Figure 5.9 shows the Strouhal number versus fully expanded jet Mach number for single jet. The other curve in figure 5.9 was plotted by using Crocco's relation [18],

$$St = 0.67(M_j^2 - 1)^{-1/2}[1 + 0.7M_j(1 + \frac{\gamma - 1}{2}M_j^2)^{-1/2}(\frac{T_a}{T_r})^{-1/2}]^{-1} \qquad (5.6)$$

In equation 5.6, T_a / T_r is the ratio of ambient to reservoir temperature of the jet. This equation is valid for hot as well as cold single jets. As can be seen, the agreement between the equations 5.5 and 5.6 and the experimental measurements are good. Since the frequency of the screech tone is dependent on the shock cell length , the screech frequency and Strouhal number decrease as the jet Mach number and shock cell length increase.

c) Acoustic Wavelength

Wavelength is the distance measured perpendicular to the wave front in the direction of propagation between two successive points in the wave, which are separated by one period. Having measured screech frequency f_s, the acoustic wavelength λ can be calculated as follow,

$$\lambda = \frac{a_o}{f_s} \qquad (5.7)$$

where a_o is ambient sound velocity.

The data are presented in terms of acoustic wavelength, λ, normalized by the internal tube diameter D. Figure 5.10 shows the dependence of λ/D on M_j is

generally linear. As shown, several modes exist, and sometimes appearing simultaneously. Each jet develops an axisymmetric mode at low M_j, and helical modes at higher M_j. This is in good agreement with previous work [4,6,8]. Since the frequency of the screech tone is dependent on the

shock cell length, the screech tone frequency decreases or acoustic wavelength increase as the jet Mach number and shock cell length increase.

d) Sound Pressure Level

Sound pressure level is defined as

$$SPL = 20\log\frac{p}{p_o} \tag{5.8}$$

where p is the root mean square, *RMS*, value of sound pressure in Pascals and p_o is 20μ Pa for measurement in air.

The sound pressure levels of different modes are presented in figure 5.11 as a function of M_j for single jet. When two helical stages (*B* and C)are present, increasing the level of one the stages causes reduction in the other. This is only noted in the early stage of formation of the *C* mode. The helical modes are dominant for $M_j > 1.32$, and maximum sound pressure 152 dB was obtained at M_j =1.470. These modes were defined in details in references [33,34].

e) Pressure Amplitude

Having measured sound pressure level, the dynamics pressure amplitude can be calculated from equation 5.9

$$p = (\frac{SPL}{20})^{10} p_o \tag{5.9}$$

Figure 5.12 shows pressure amplitude as a function of fully expanded jet Mach number M_j .The dashed line near 1100 Pa represents a reference level above which sonic fatigue and crack growth problems can usually be expected for aircraft metallic type structures [36] . It is observed that over the range of study, the pressure amplitude of single jet did not reach this reference level.

5.2.2 Twin-jet Results

Similar tests were carried out by using three different twin-jet models with centre-to-centre spacing of 1.6, 1.8, and 2.0 times the tube diameter. The results illustrate the difference between single and twin jets screech tones, and the effect of the nozzle spacing on the screech tone frequency and amplitude of the twin-jet.

Typical spectra from single and twin-jet (S/D=2.0) are shown in figure 5.13. These spectral records were obtained for the underexpanded jet at a pressure ratio 2.905 corresponding to the fully expanded Mach number 1.335 and spectral data show the high-amplitude screech tone with the first harmonic tone. The fundamental screech tones for single and twin-jet are at 11.4 KHz and 10.9 KHz, respectively. They differ slightly in frequency because the twin-jet results in an increase in shock cell length causing a lower screech tone frequency. This result is in good agreement with optical result. However the screech tone amplitude of twin-jet is about 12.3 dB higher than the single jet at this particular jet Mach

number.

Typical spectra from three twin-jet models are presented in figure 5.14. As it was expected from the optical results, the screech tone frequencies of different twin-jets must be almost equal.They are around 11.2 KHz, however the amplitudes are 146 dB, 150 dB, and 154 dB for S/D=1.6, 1.8, 2.0 models, respectively. Therefore, the spacing significantly effects the screech tones amplitudes.

a) Screech Tone Frequency

Frequencies of the three twin-jets can be written in terms of the Strouhal numbers. Figure 5.15 shows the Strouhal number as a function of jet Mach number for three twin-jet models. The results of spacing effect on screech frequencies are summarized in figure 5.16. By combining equations 5.3 (optical results), and 5.4 , equation 5.10 can be obtained to predict the twin-jet frequency screech

$$St = \frac{0.7(D_j/D)}{1.17(M_j^2-1)^{1.36}(1+M_c)} \qquad (5.10)$$

b) The Acoustic Wavelength

The acoustic wavelength for each twin-jet model is presented in figure 5.17. By compression these results and the single jet wavelength results in figure 5.10 it is found that all three stages *A,B,* and *C* never appear simultaneously in twin-jet.

c) Sound pressure levels

Figure 5.18 shows the sound pressure levels as a function of jet Mach

number. For the minimum spacing, S/D=1.6, the helical modes are dominant for $M_j > 1.28$. The average *SPL* in this range is about 4 dB higher than that of single jet (figure 5.18a), and the maximum *SPL* is 155.2 dB at M_j =1.569. For spacing S/D=1.8, the helical modes dominate for $M_j > 1.26$, and average *SPL* is 4.4 dB higher than that of twin-jet with spacing S/D=1.6 (figure 5.18b). The maximum sound pressure level recorded is 155.2 dB at $M_j = 1.414$. The sound pressure level of maximum spacing is presented in figure 5.18c. For $M_j > 1.26$ the helical modes are dominate, and the average *SPL* is 1.5 dB higher than that of previous model. The maximum *SPL* measured is 155.7 dB at M_j =1.335. Therefore, as seen from figure 5.18, the screech tone amplitudes depend on the jet spacing, and are significantly increased as the spacing is increased.

The results of spacing effect on the screech tone amplitudes for single and twin jets are summarized in figure 5.19. The shown levels are for the maximum screech tone.

d) Pressure Amplitude

By using equation 5.9 the pressure amplitude for three models were obtained. The results are presented in figure 5.20. The dashed line presents a reference level above which sonic fatigue can usually be expected. As seen , the pressure amplitude of the three twin-jet models exceed the reference level, however the pressure amplitudes of twin-jet with spacing S/D=1.6 are high only at elevated jet Mach numbers. Therefore close spacing can be considered as a

technique to suppress the level at low and middle jet Mach number.

5.3 Suppression of The Screech Tone Amplitude

As previously mentioned, the pressure amplitude of twin-jets can exceed the reference sonic fatigue level [35]. The second objective of this study was to examine a method to reduce the pressure amplitude.

The effect of multiple tabs (up to 4) was investigated in the current study. A sketch of the tab is shown in figure 5.21 along with a typical installation on the tube. The tabs were attached to the outside of the tube with only the tapered portion of the tab in the flow, resulting in about 1% of the nozzle exit area per tab, therefore, these tabs don't involve significant loss of nozzle's thrust.

Since twin-jet with spacing S/D=2.0 generated the screech tones of highest amplitudes, this model was selected for suppression testing by tabs. Flow visualization photographs of the multi-tab are presented in figure 5.22. As noted in the figure, the tabs reduce the shock cell length and distort the cell structure. They also weaken the strength of oblique shock waves, as seen in figure 5.22c, where the darkness of the oblique shock wave has almost vanished. Typical spectra with suppression and without is shown in figure 5.23. At this jet Mach number M_j = 1.368, suppression as much as 7 dB can be achieved by using 4 tabs. When more than one screech mode is present , suppression of one mode may amplify the other. This amplification, however, never reaches the fatigue sonic level (figure

5.24)

Figure 5.25 shows the suppression levels of 4 tabs. Suppression is based on the amount of reduction in the peak mode without regard to which mode it is. One and two tabs result in the least suppression. Three tabs yield better results than four tabs at higher Mach number, however 4 tabs appear to do better than 3 tabs in the mid-Mach number. Figure 5.26 shows the pressure amplitude of the twin-jet as a function jet Mach number with and without using the tabs. It can be seen that even one tab can significantly reduce pressure amplitude.

CHAPTER 6

CONCLUSIONS AND RECOMMENDATIONS

A laboratory test was performed to investigate the flow and noise of single and twin supersonic underexpanded jets. A single and three twin chocked tube models were used. The centre-to-centre nozzle spacings for the twin-jet models were chosen at 1.6, 1.8, and 2.0 times the jet exhaust diameter. Optical and acoustic data were obtained over the pressure ratio range of 2.224 to 4.061. Observations will be discussed in the following sections.

6.1.1 Optical Conclusions

A Spark schlieren system was employed to obtain optical results which demonstrated the shock cell deformation and the coupling process between the two jets. From this study, semi-empirical relations of the average shock cell length variation with jet Mach number were derived. It was found that shock cell length, for both single and twin jets, increased with jet Mach number. However, with the exception of very low jet Mach number, the average shock cell length of twin-jet was found to be greater than that of the single jet. These results were used to predict screech tone frequency using Powell's model. The results also show that the shock cell length is practically independent of centre-to-centre spacing.

6.1.2 Acoustical Conclusions

Noise spectra were obtained at 28 pressure ratios by placing a microphone at the exit plane of the nozzle and connecting it to a signal analyzer unit. The frequency and amplitude of the screech tones were determined for both single and twin jet models.

Several stages of screech tone were observed. These different stages may be attributed to frequency jumps resulting from changes in pressure ratio and shock cell length. Toroidal or axisymmetric type structure is limited to lower values of jet Mach number, and the helical structure dominates at higher Mach number. However for twin-jet configuration helical modes can dominate over a wider range.

It was found that at a given jet Mach number the screech tone frequency of twin-jet was slightly lower than that of a single jet. This result was in good agreement with the optical result which indicated that the average shock cell length of twin-jets is greater than that of single jet. Unlike small differences in screech tone frequencies, significant differences in screech tone amplitudes of single and twin jets were obtained. The average twin-jet screech tone amplitudes were found to be greater than that of single jet over range of study. The significant increase of twin-jet amplitude may be caused by the coupling process of two close supersonic jets which support the helical modes.

The effect of different centre-to-centre spacings of twin-jets was analyzed. The screech tone frequencies of three twin-jet configurations were found to be

almost the same at a given jet Mach number. The screech tone amplitude was, however, observed to be largely dependent on the jet spacing. Larger jet spacing produced higher amplitudes. Smaller spacing supported the axisymmetric mode and let two plumes merge before developing the helical modes. The results demonstrated that the coupling process mechanism is complex, and that relatively small changes in nozzle spacing can have a noticeable effect on the screech tone amplitudes. The pressure level recorded for twin-jet configurations exceeded the reference level of sonic fatigue for aircraft metallic type structures. Therefore, structural damage found in supersonic twin-jet configurations may be caused by this high pressure amplitude .

Small rectangular tabs, placed in the flow at the exit plane of the nozzle, were found to be very effective in suppressing the screech tone amplitude. These tabs reduced the shock cell length of one of the plumes. Twin-jet screech tone amplitudes were found to be effectively suppressed using three tabs. Additional tabs were not found to have any significant effect on noise reduction except for very high jet Mach number.

6.2 Recommendations

As previously mentioned, nozzle shape modification using tabs can suppress the screech tone amplitude. Future studies of twin-jets should include the design of a nozzle shape which can produce underexpanded jets with weaker and

nonuniform oblique shocks. The fixed axial wavelength, due to the symmetry of the shock, is believed to be the cause of the high screech tone amplitudes noted at the resonant frequencies.

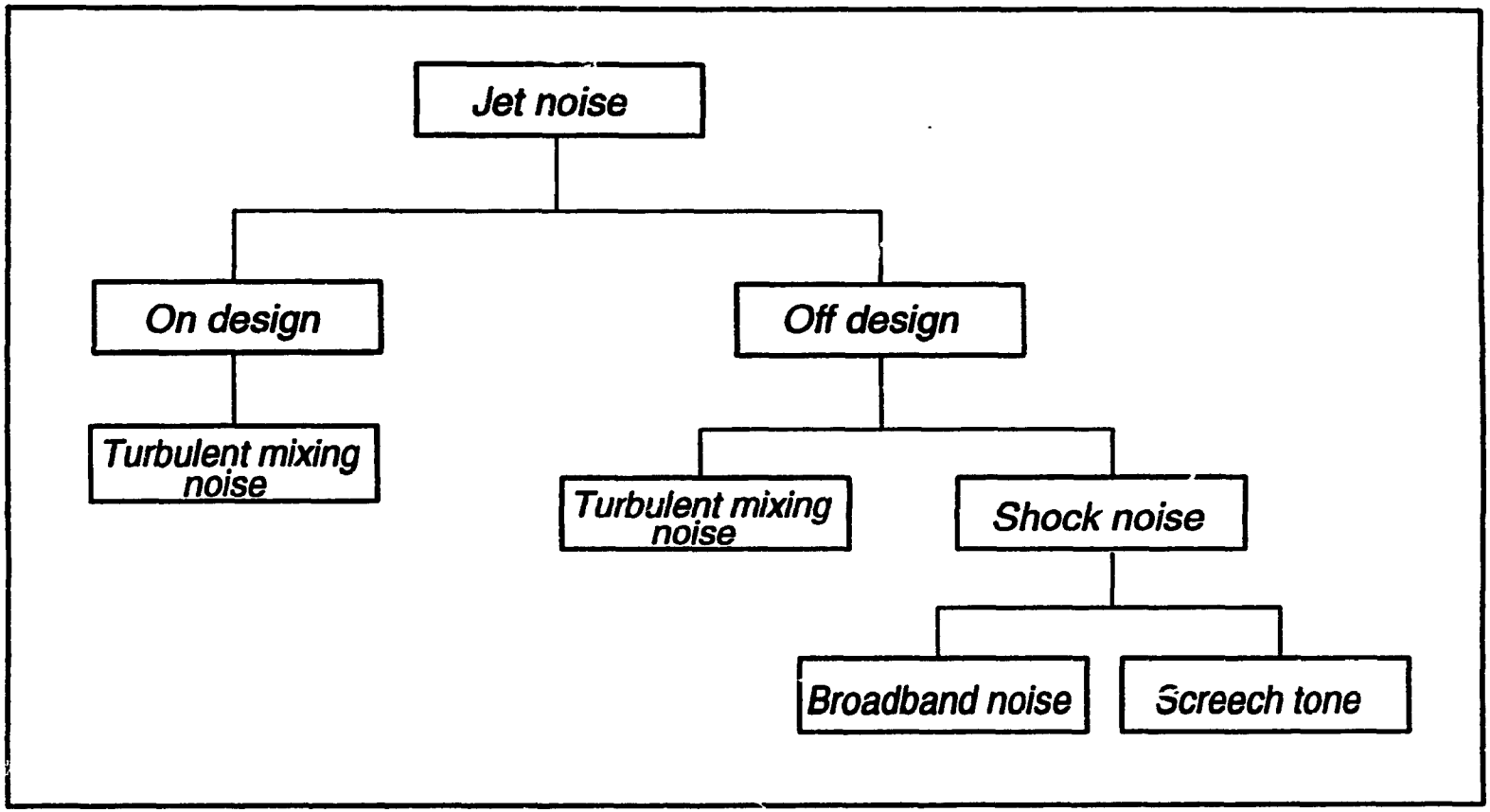

Figure 1.1 Schematic of different kinds of noises

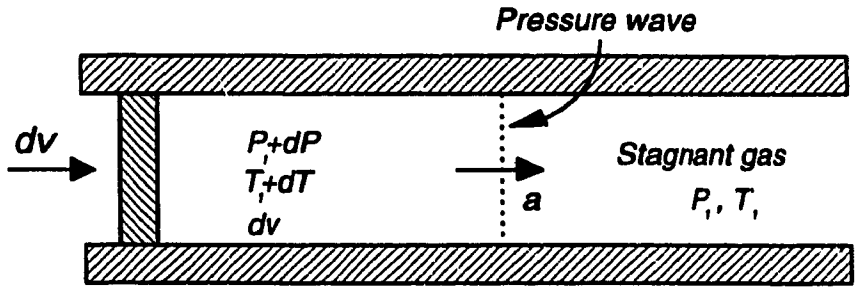

Figure 2.1 Propagation of an infinitesimal wave in a constant area duct

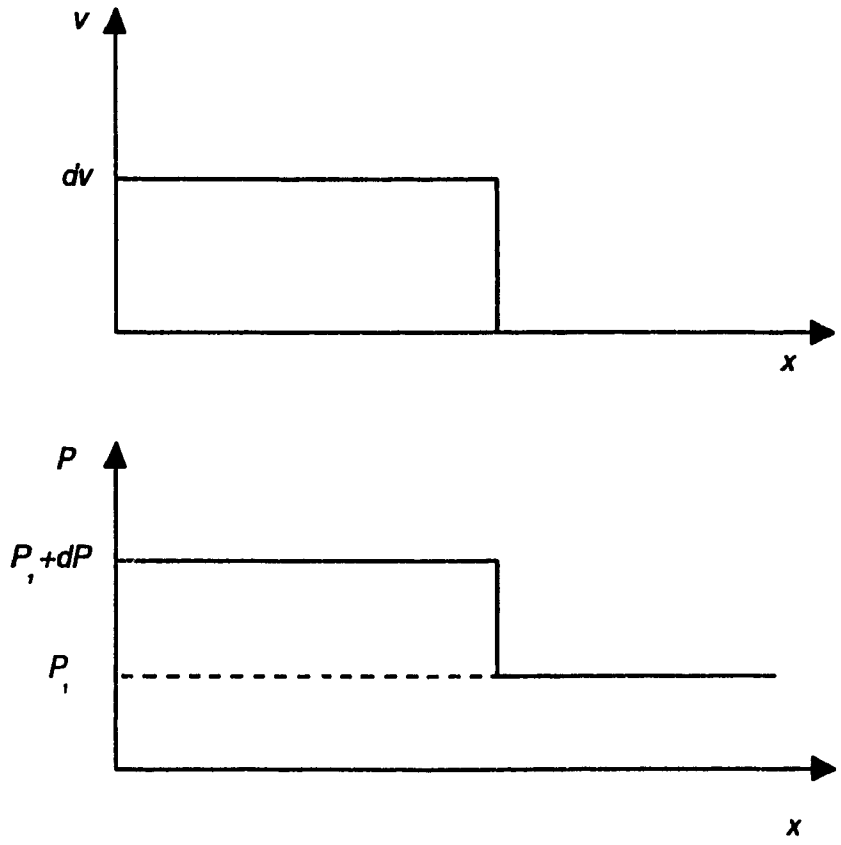

Figure 2.2 Compression wave in the direction of piston motion

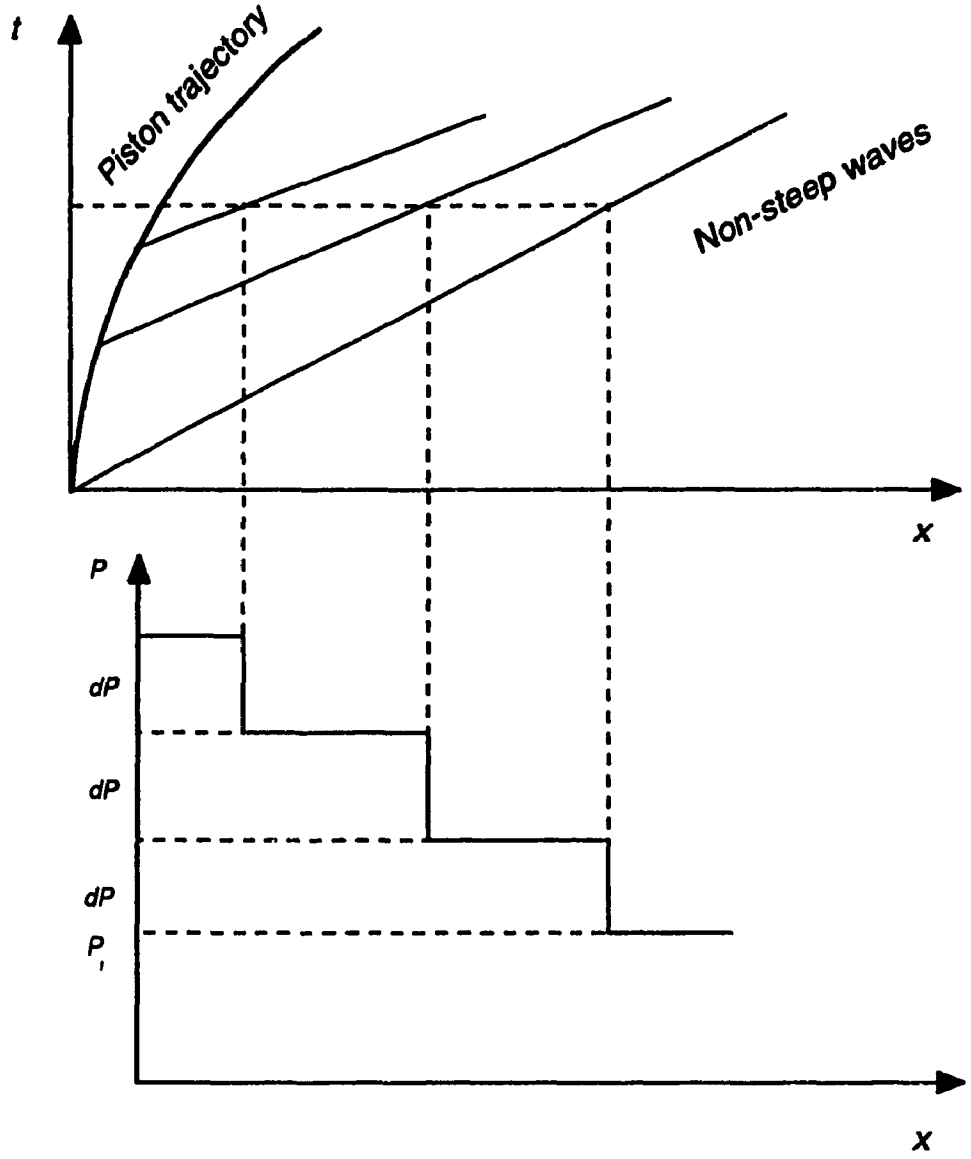

Figure 2.3 Propagation of non-steep finite compression waves

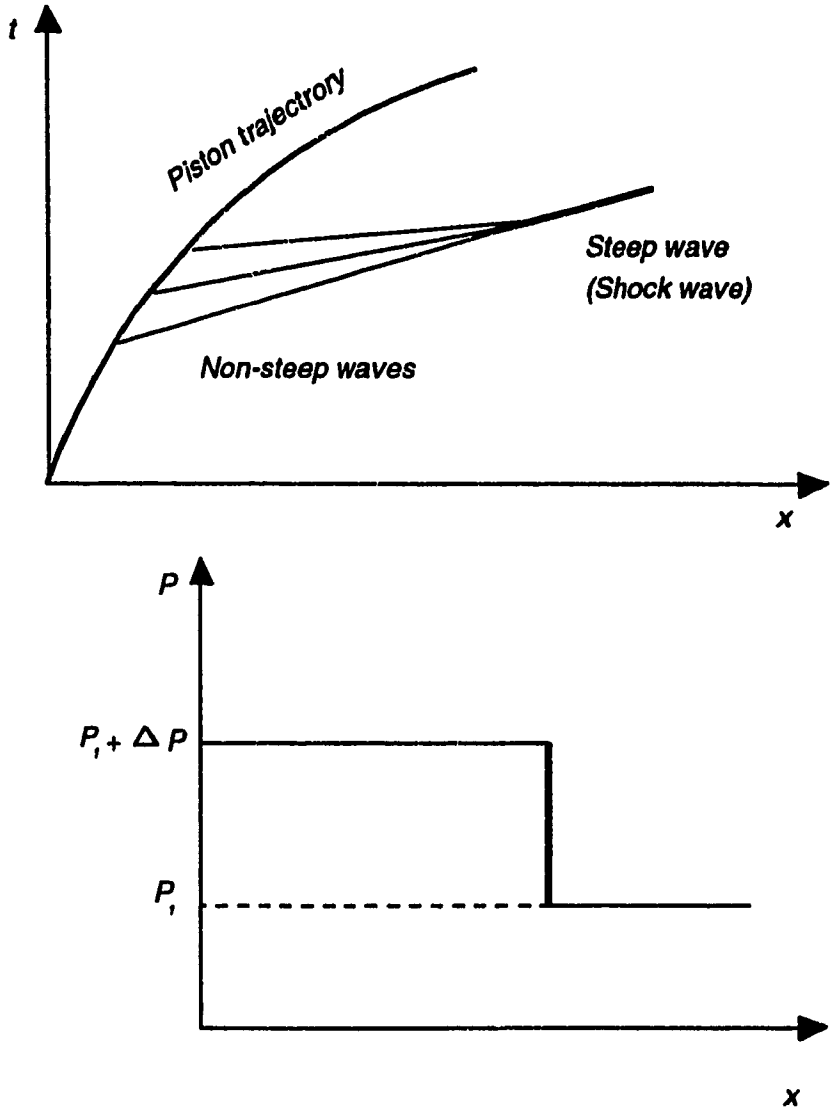

Figure 2.4 Propagation of a finite pressure steep wave (shock wave)

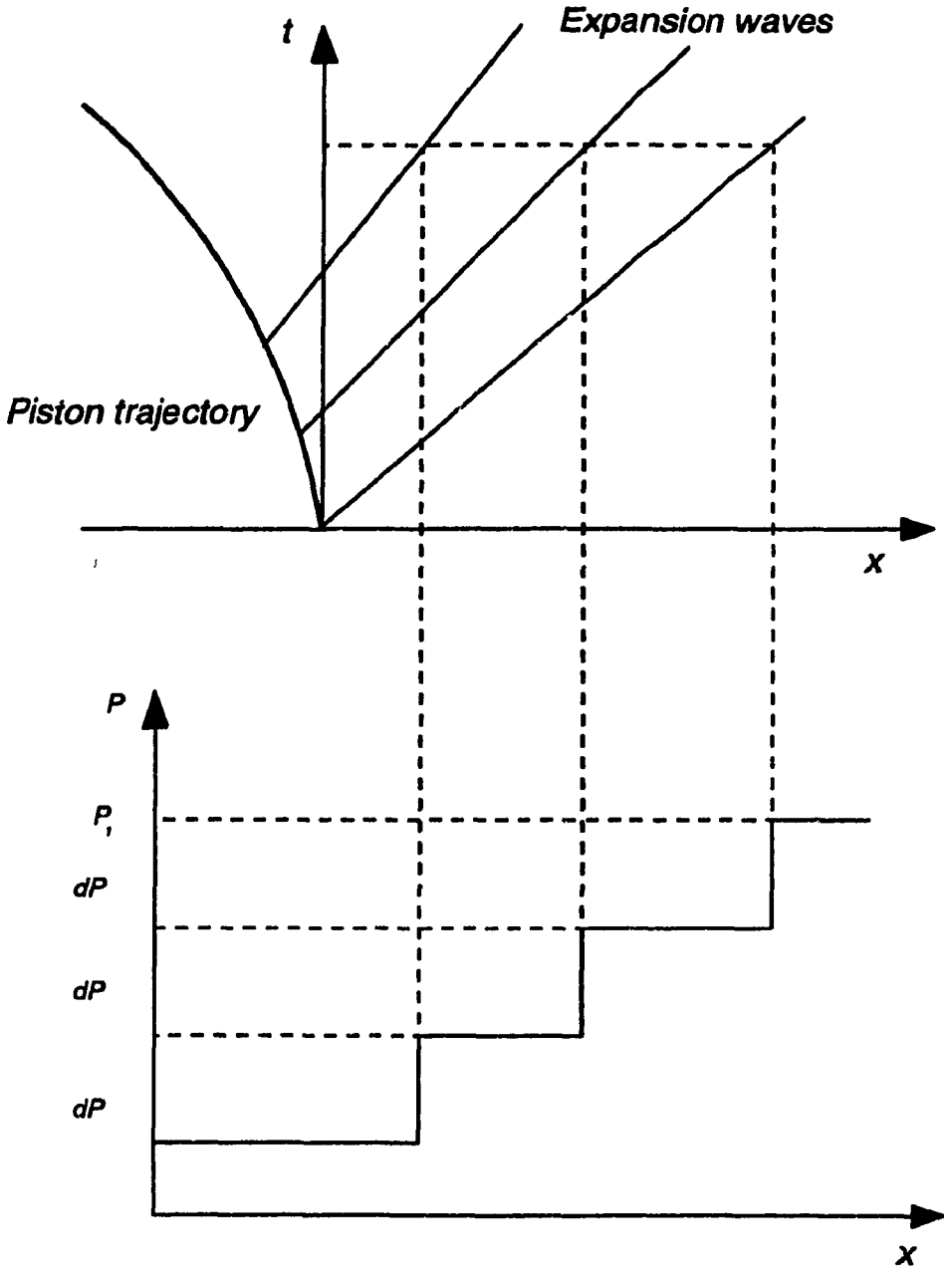

Figure 2.5 Propagation of non-steep finite expansion waves

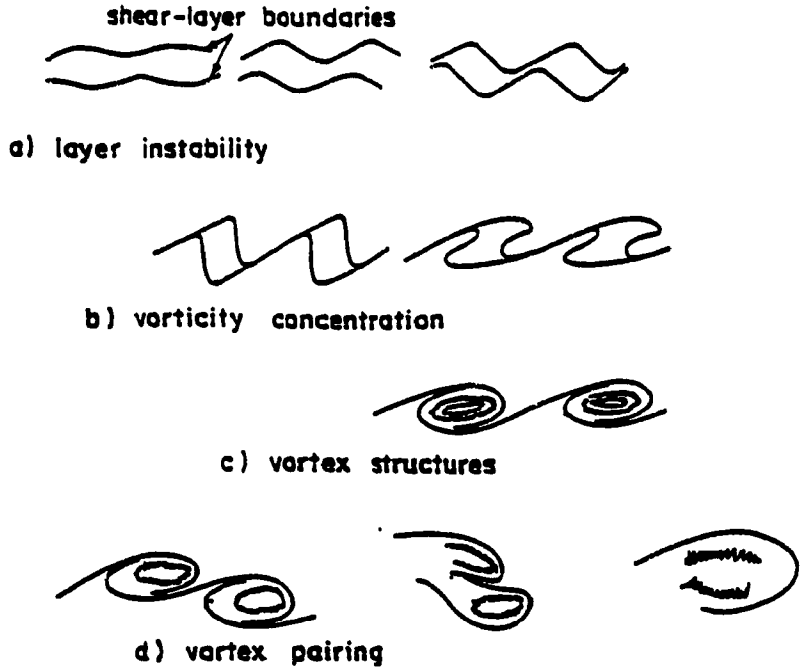

Figure 2.6 Schematic of vortex development [10]

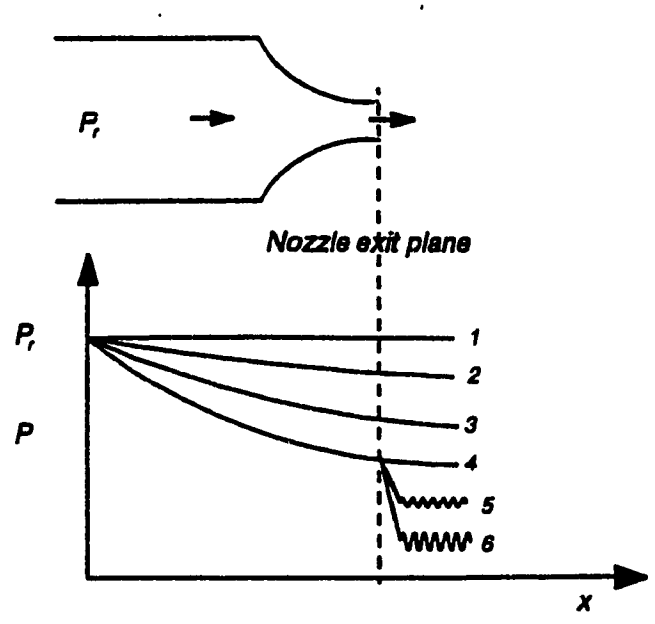

Figure 2.7 Pressure distribution in a converging nozzle

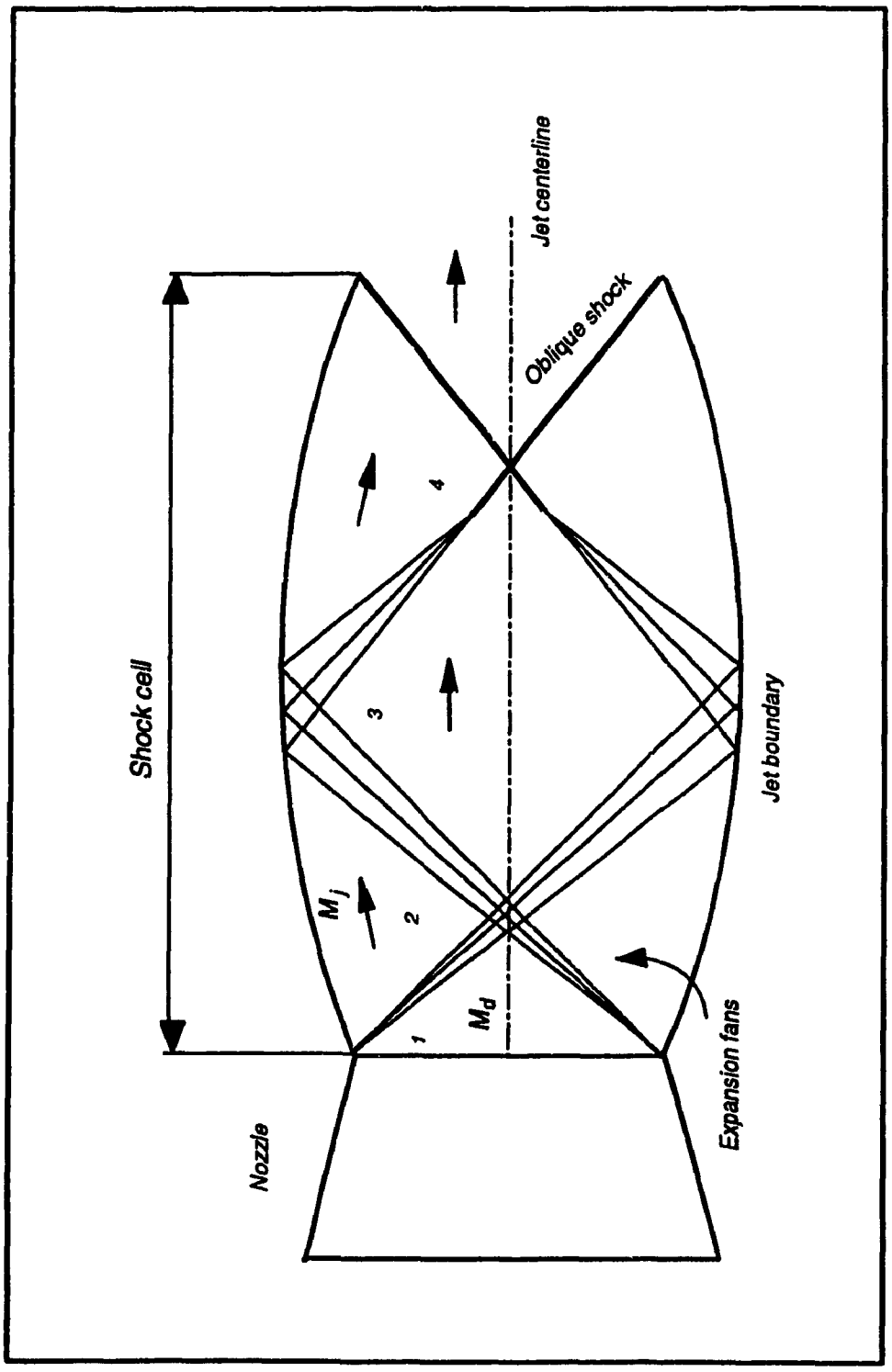

Figure 2.8 Schematic of supersonic underexpanded jet

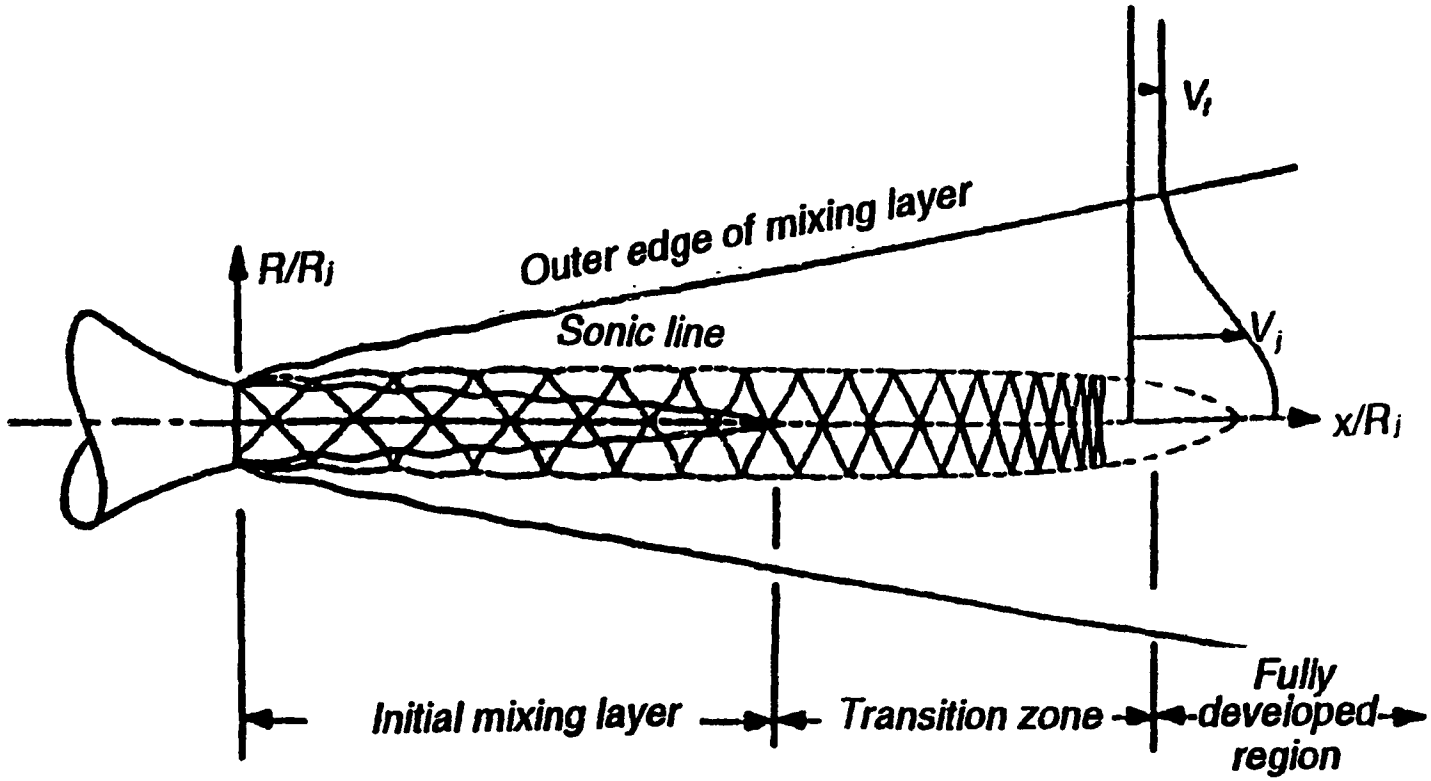

Figure 2.9 Schematic of general supersonic plume [13]

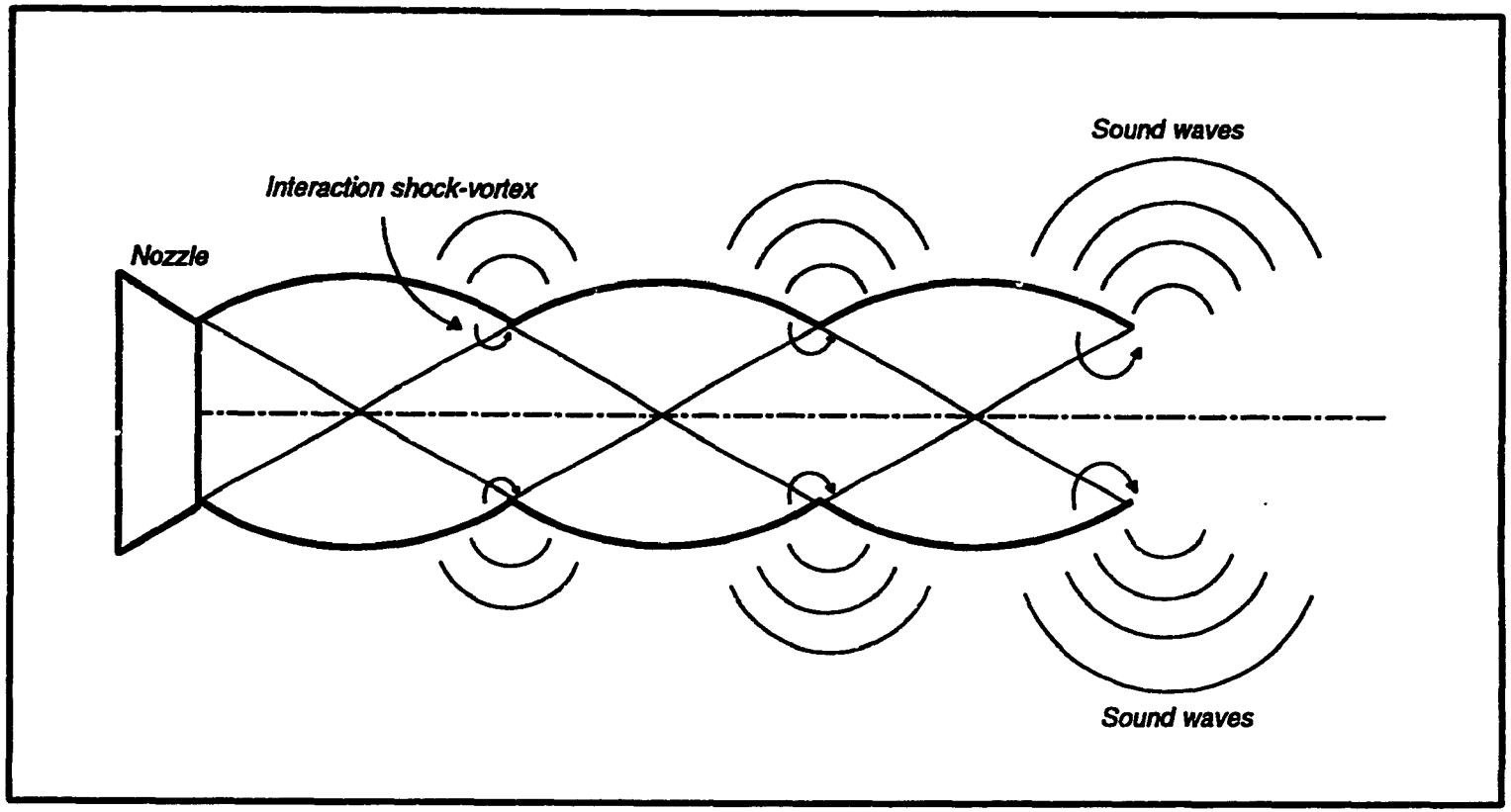

Figure 3.1 Generation of shock associated noise

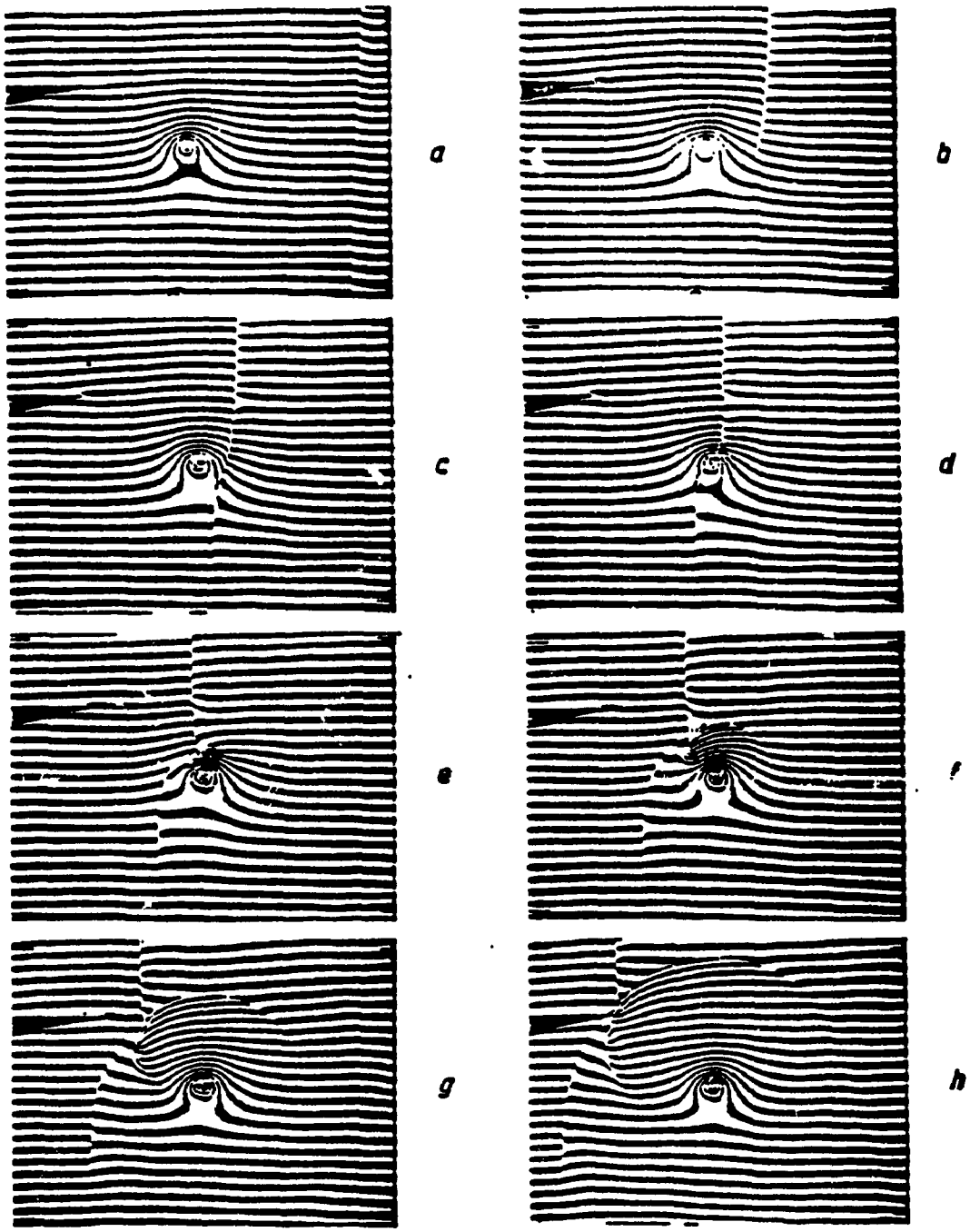

Figure 3.2 Interferograms of the interaction shock-vortex [15]

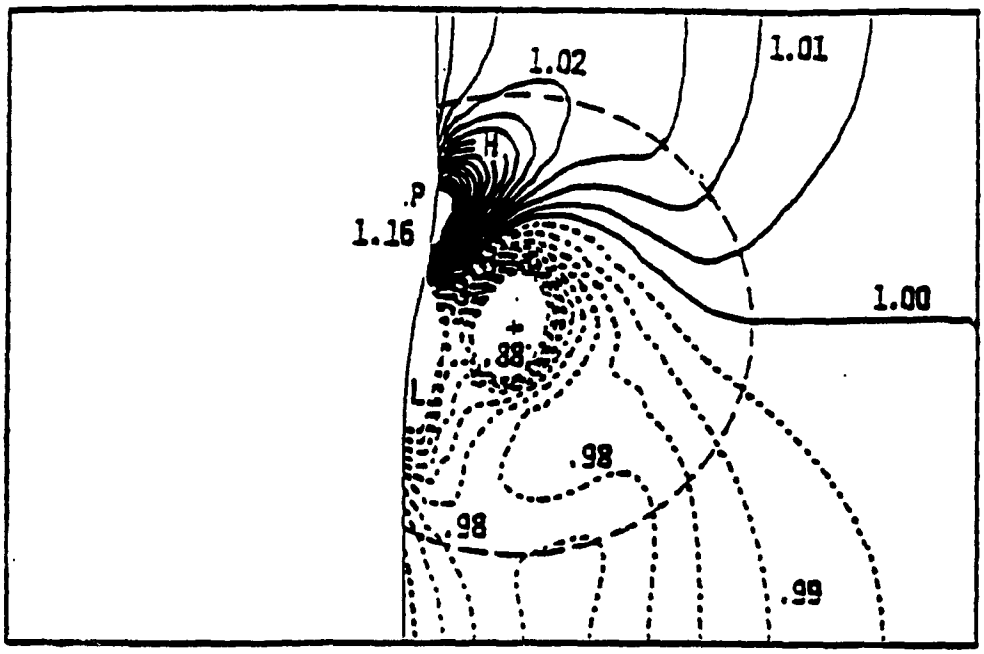

Figure 3.3 Typical computed pressure contours for shock-vortex interaction in two dimensions [14]

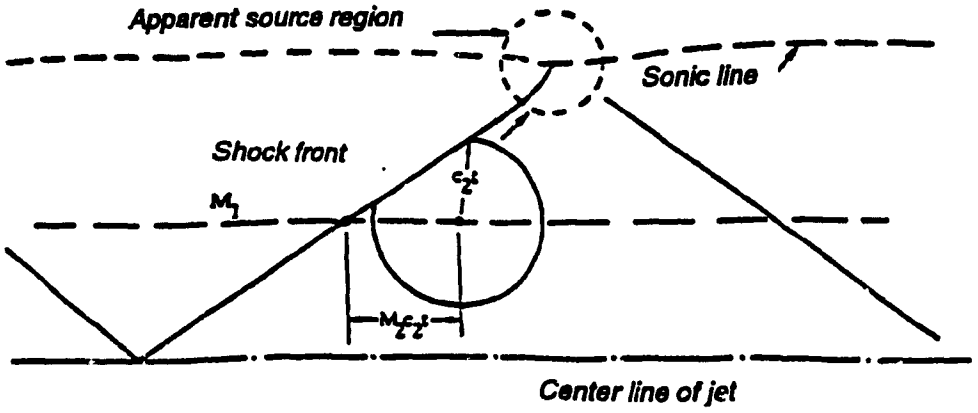

Figure 3.4 Sound source location [14]

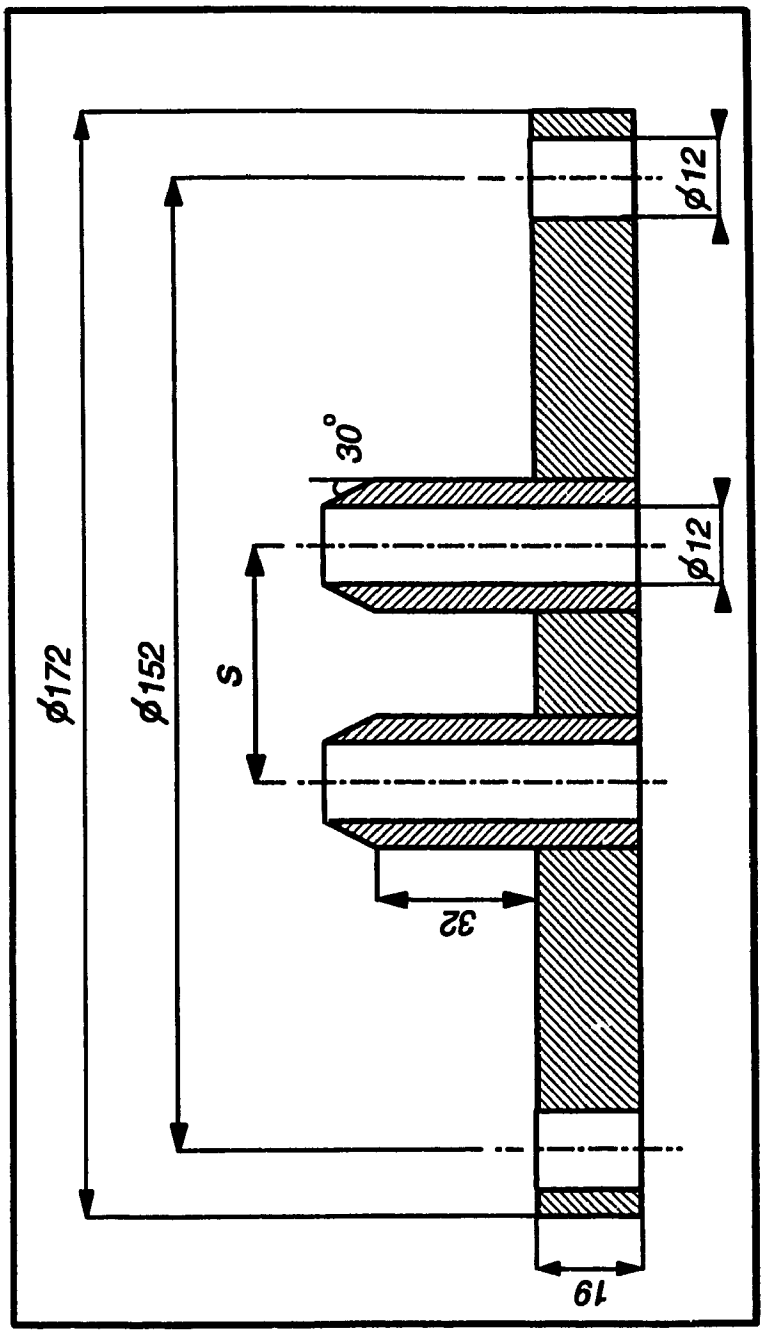

Figure 4.1 Sectional view of twin-chocked tube model (Dimensions in mm)

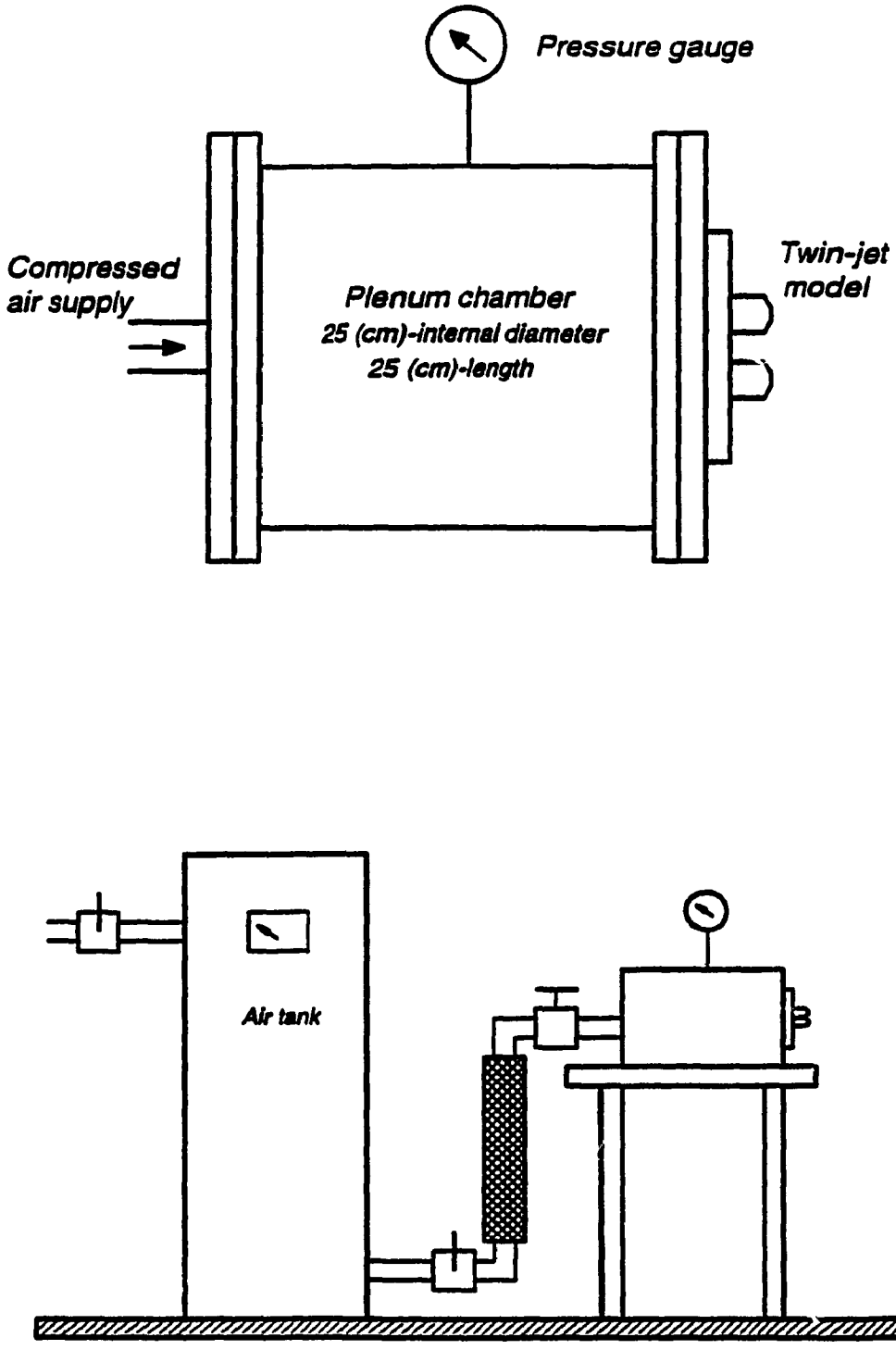

Figure 4.2 Experimental apparatus and air system

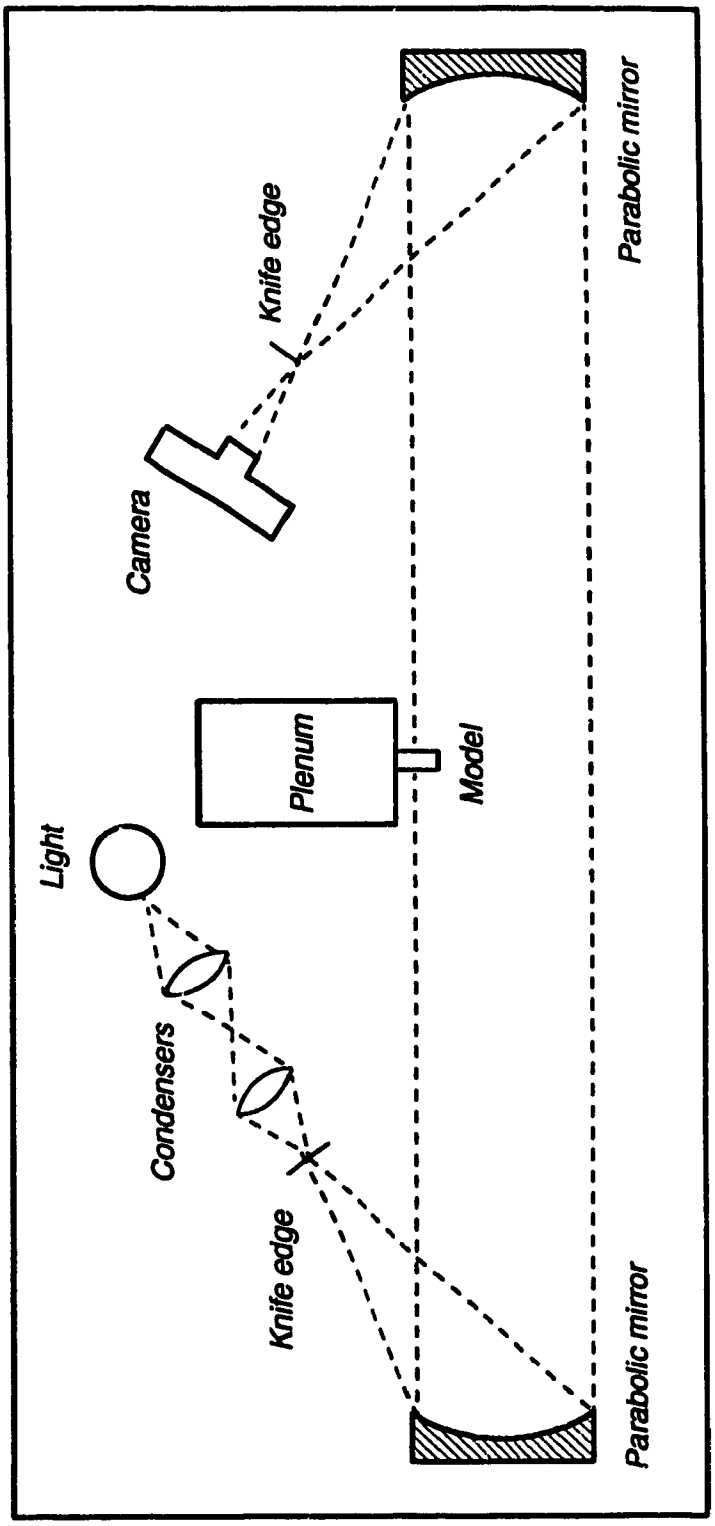

Figure 4.3 Top view of schlieren system (optical setup)

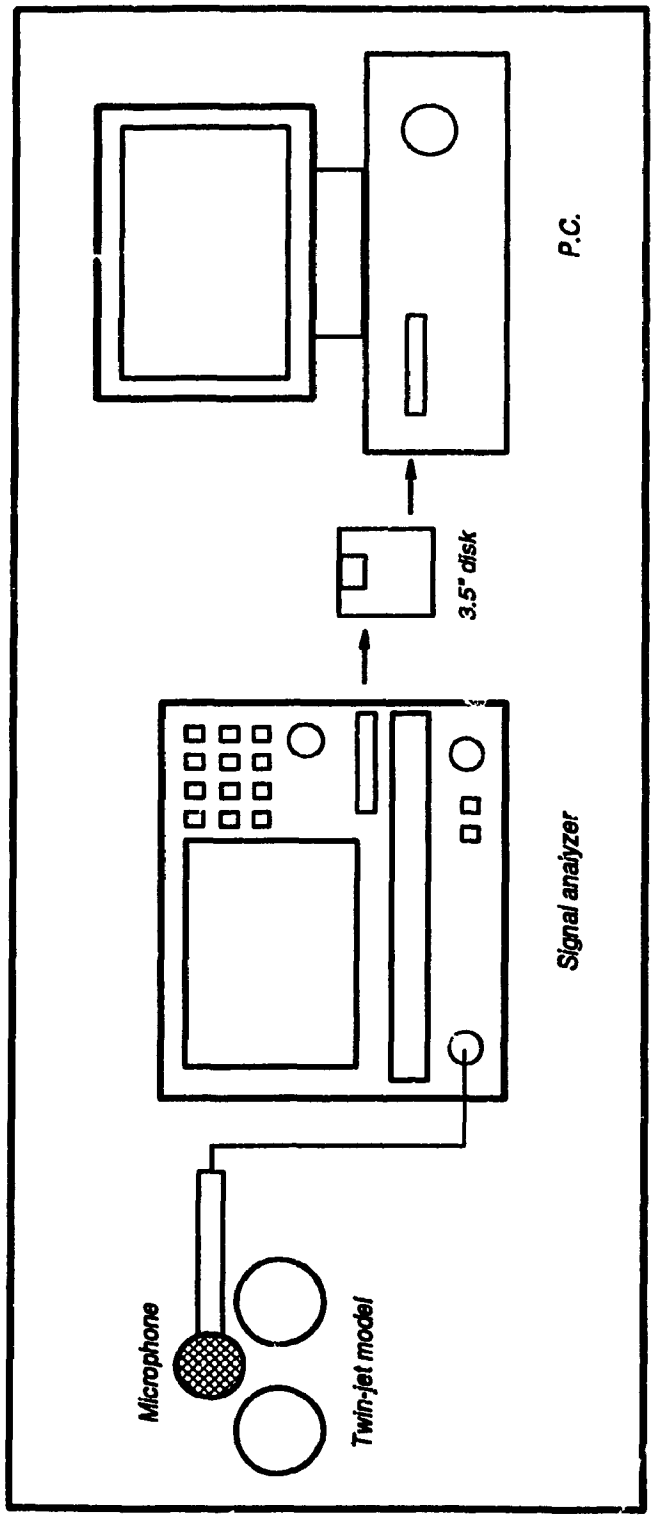

Figure 4.4 Experimental setup for noise measurements

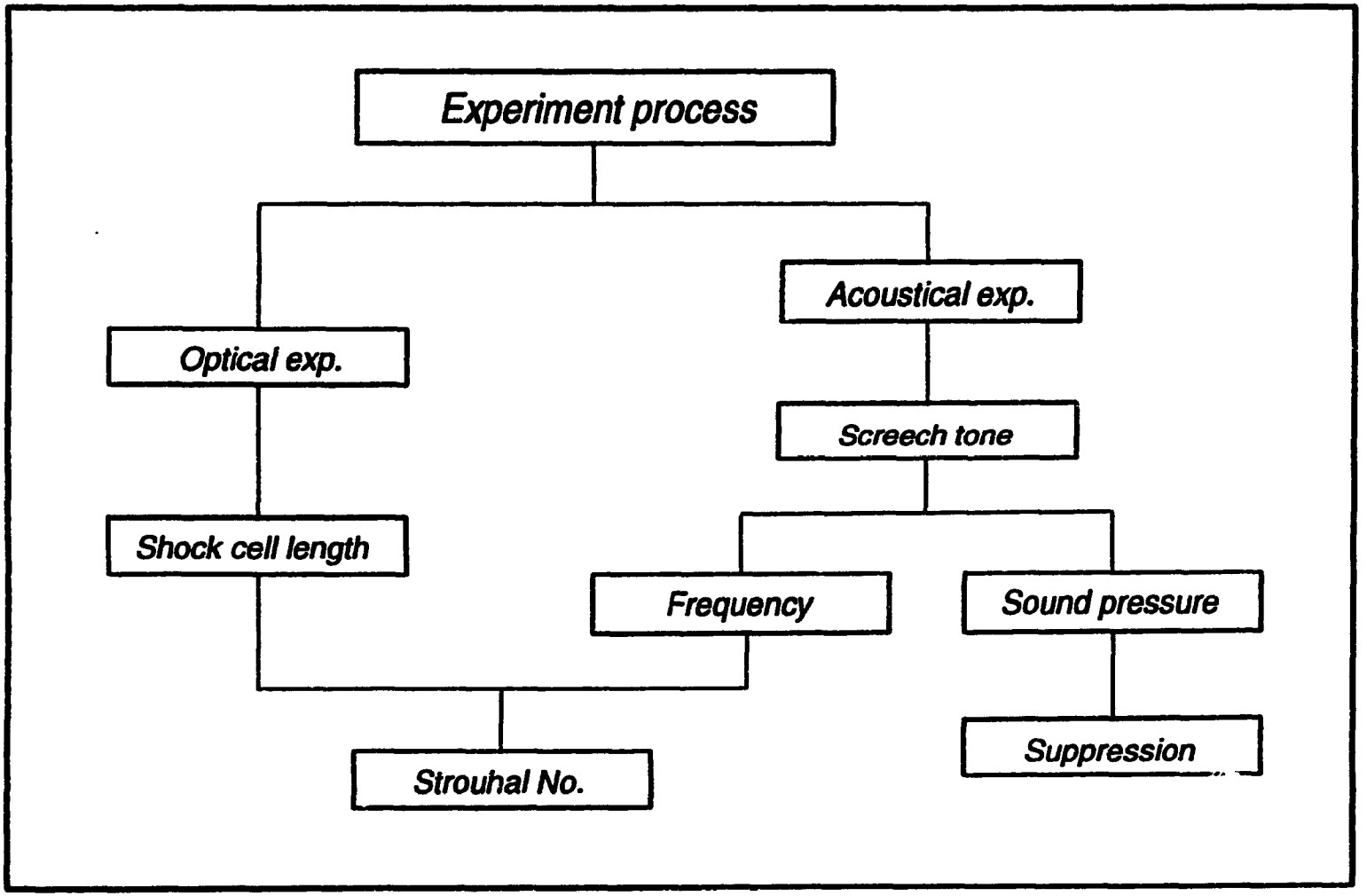

Figure 5.1 Flow chart of experimental process

a) Top view

b) Side view

Figure 5.2 Helical flow of twin-jet

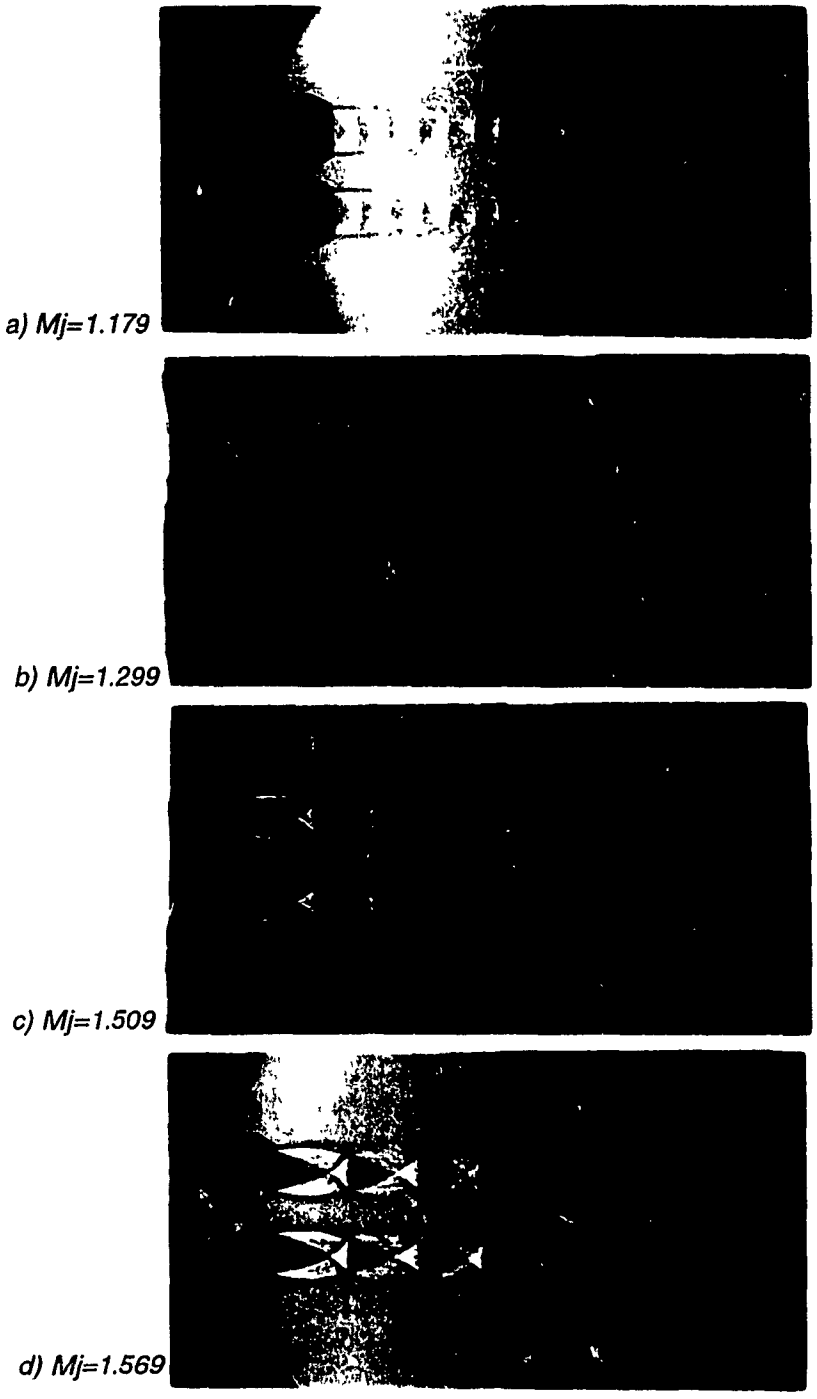

Figure 5.3 Variation in shock cell length with jet Mach number

a) Single jet

b) Twin-jet

Figure 5.4 Effect of configuration on shock cell structure

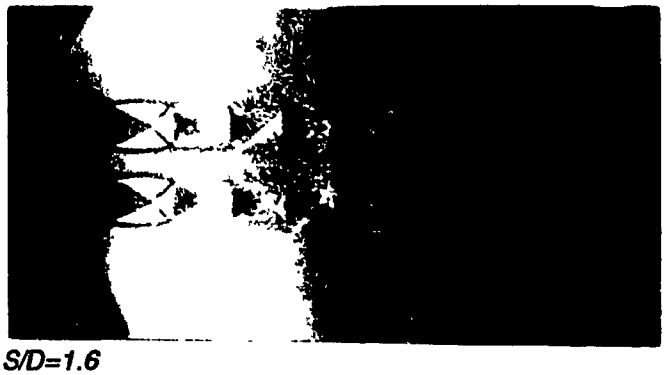

a) S/D=1.6

b) S/D=1.8

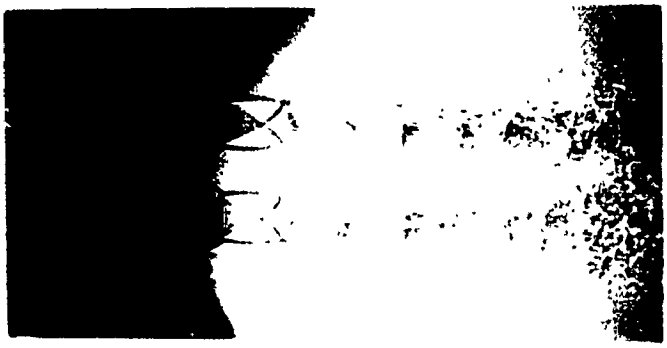

c) S/D=2.0

Figure 5.5 Effect of spacing on twin-jet shock cell structures

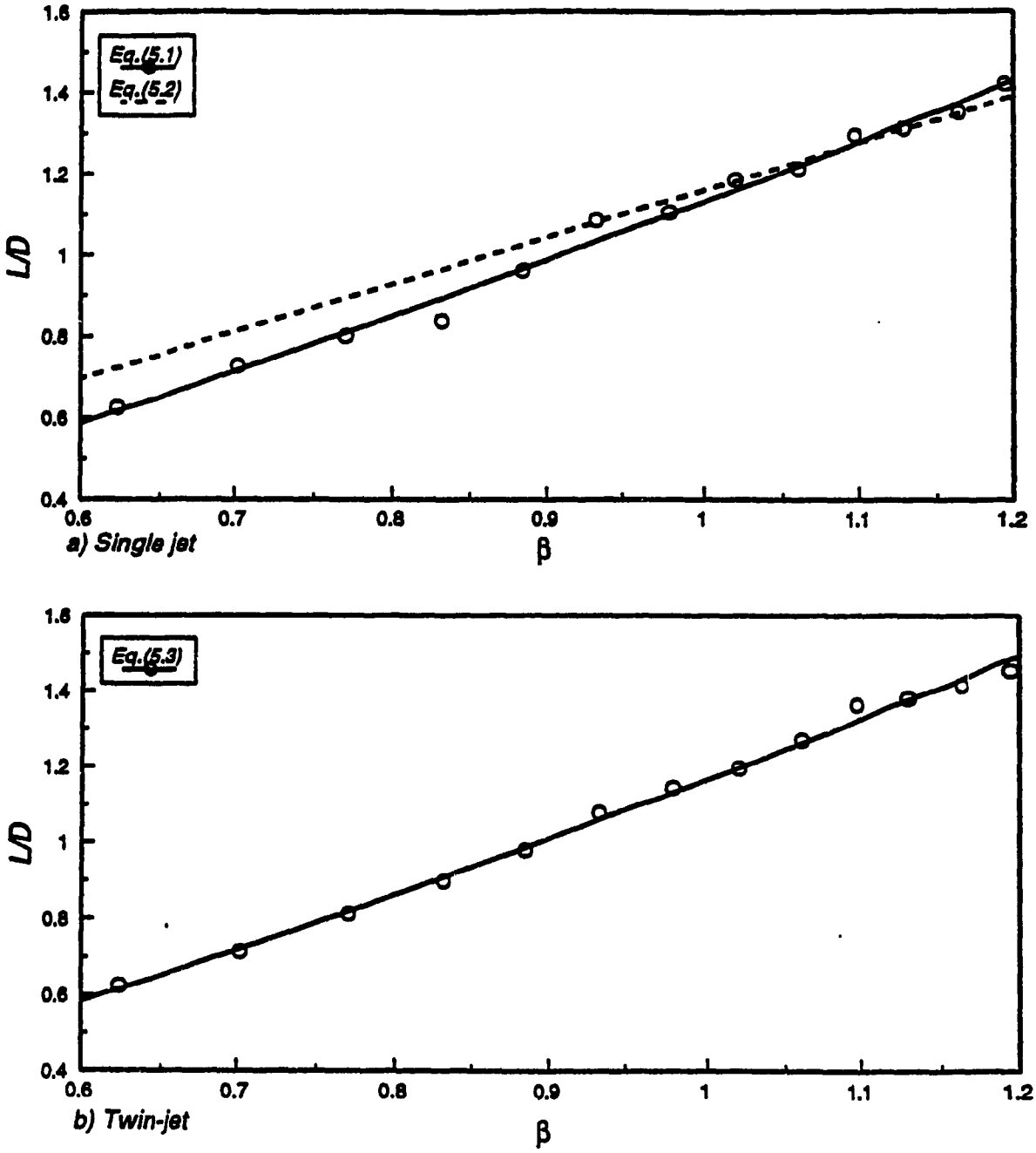

Figure 5.6 Variation in average shock cell length with β

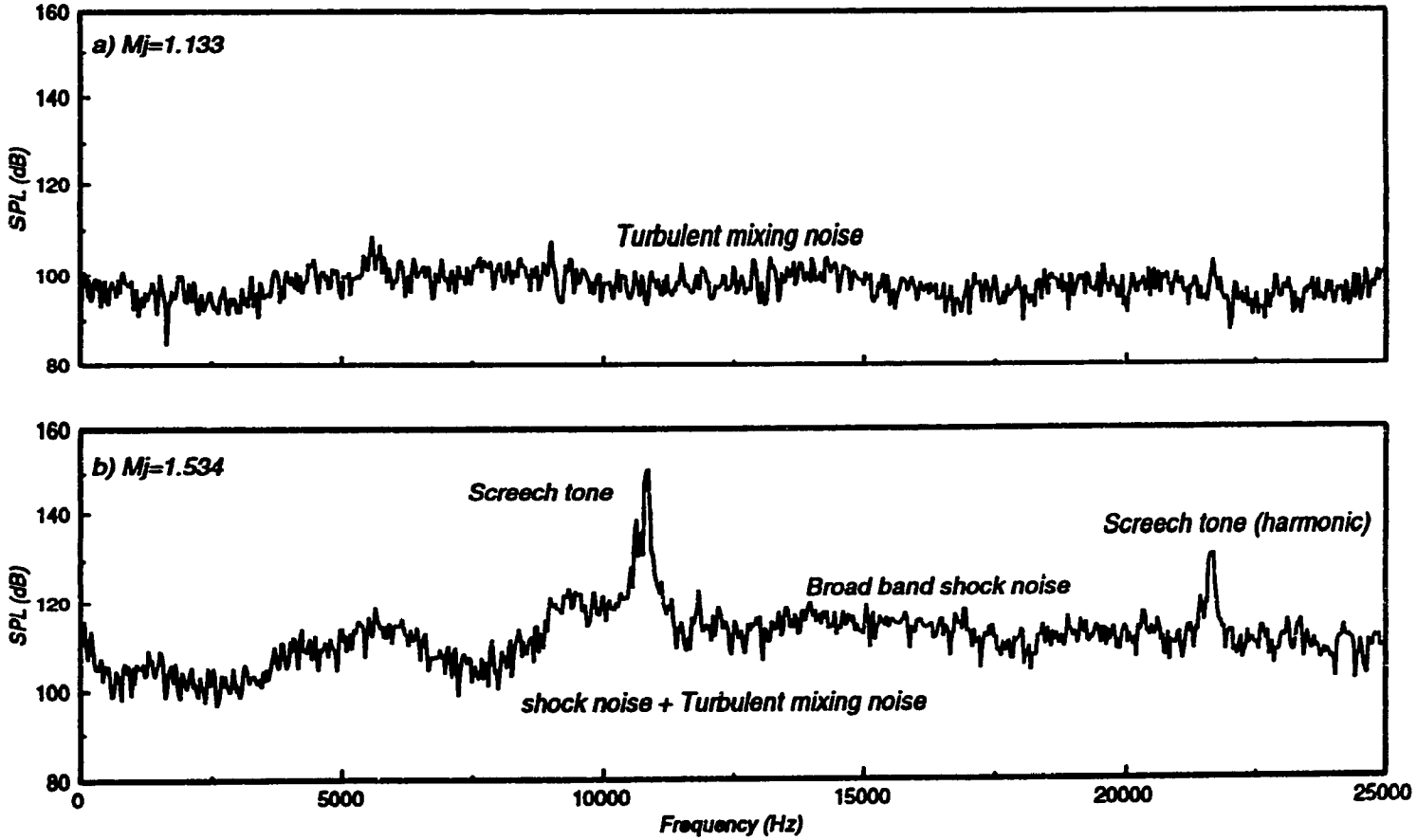

Figure 5.7 Effect of jet Mach number on noise spectra for single jet

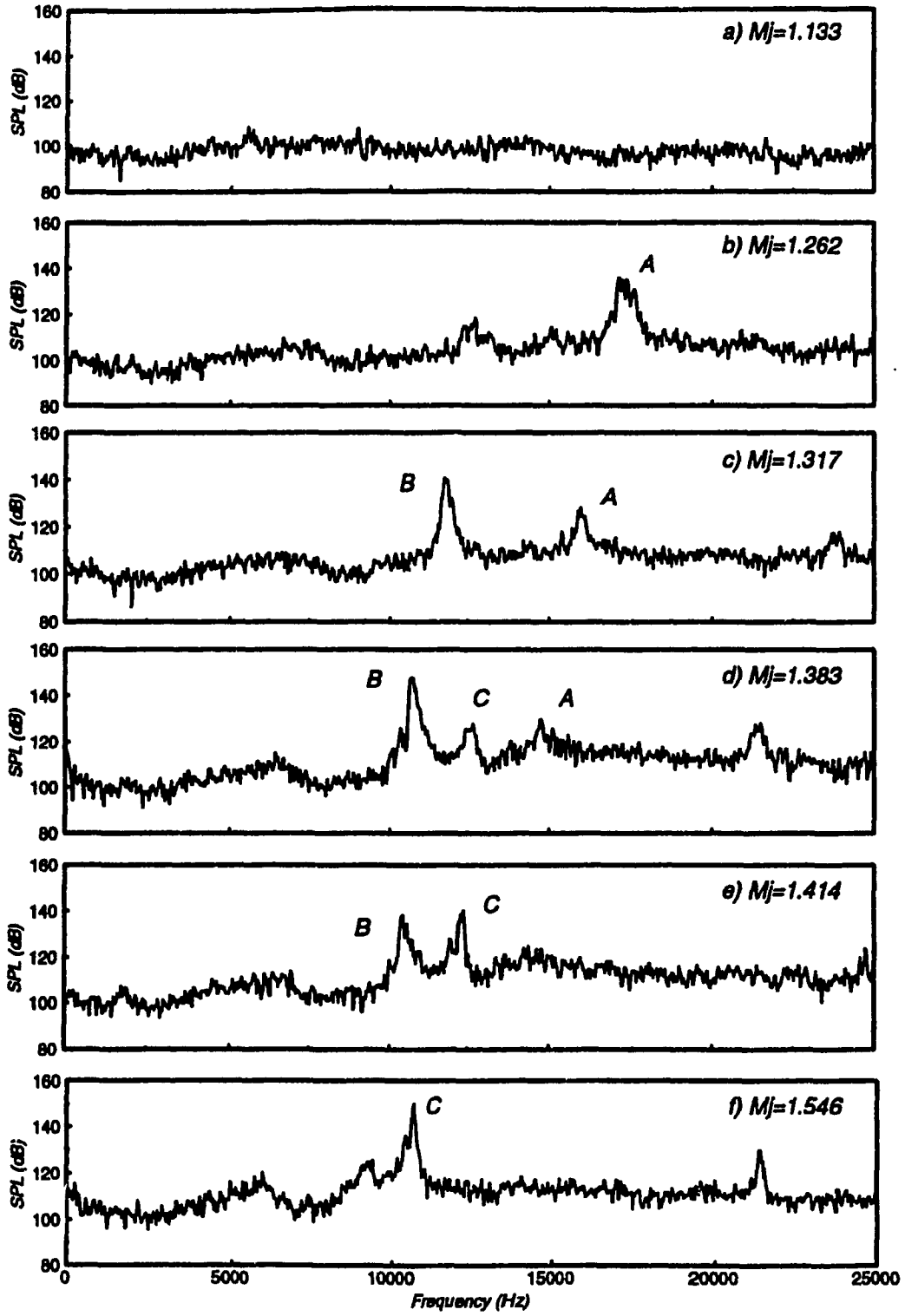

Figure 5.8 Screech tone stages for single jet

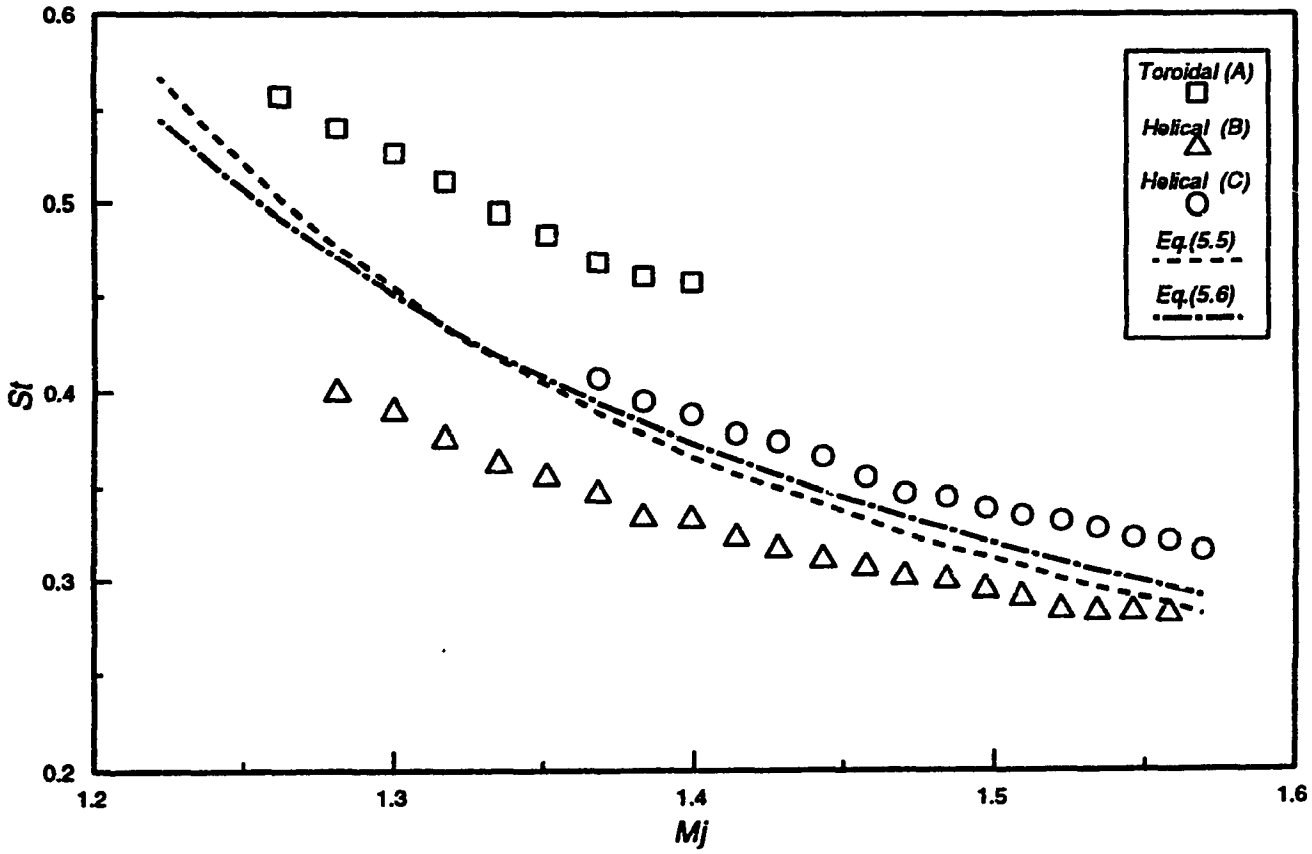

Figure 5.9 Strouhal number for single jet

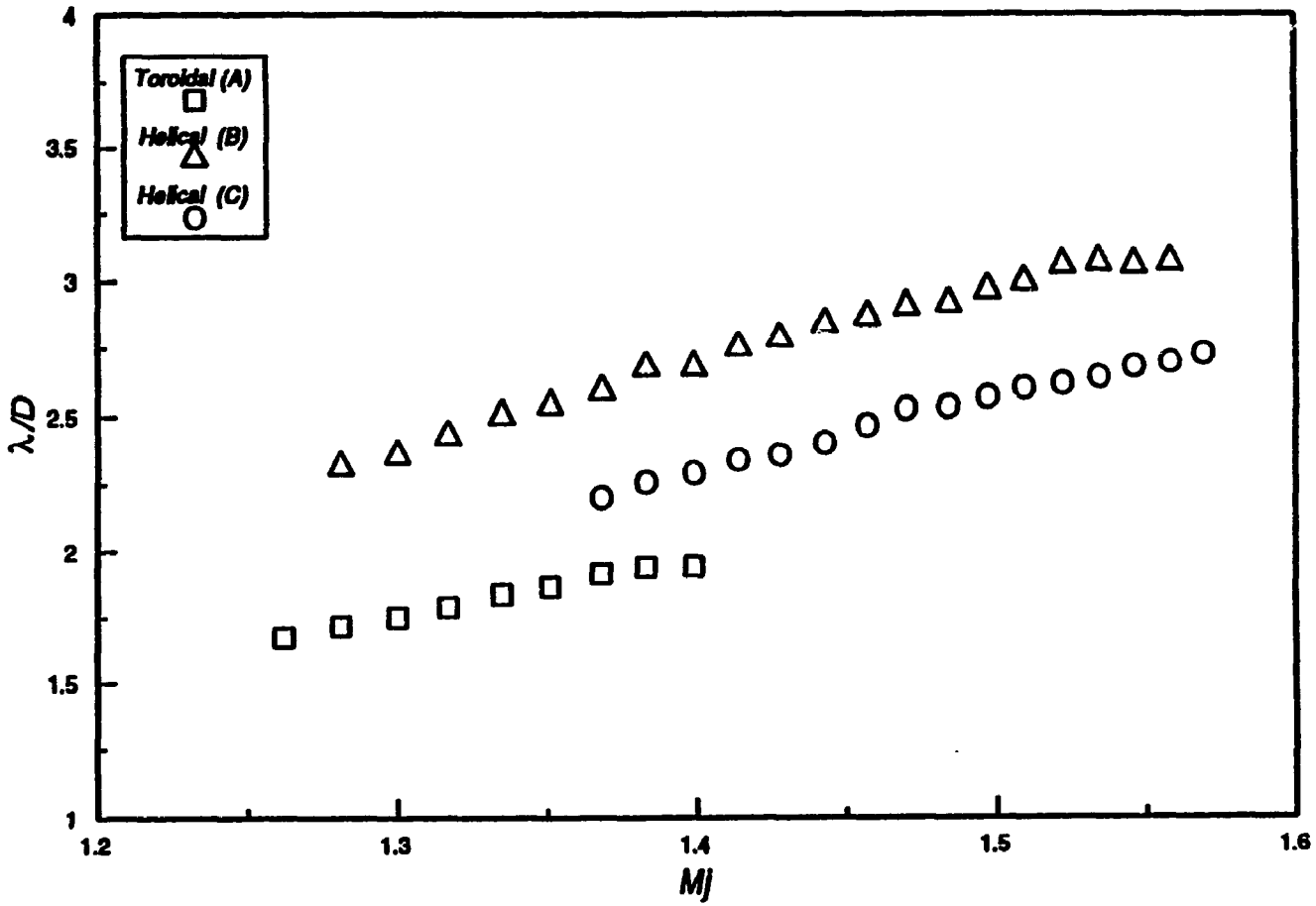

Figure 5.10 Screech tone wavelength for single jet

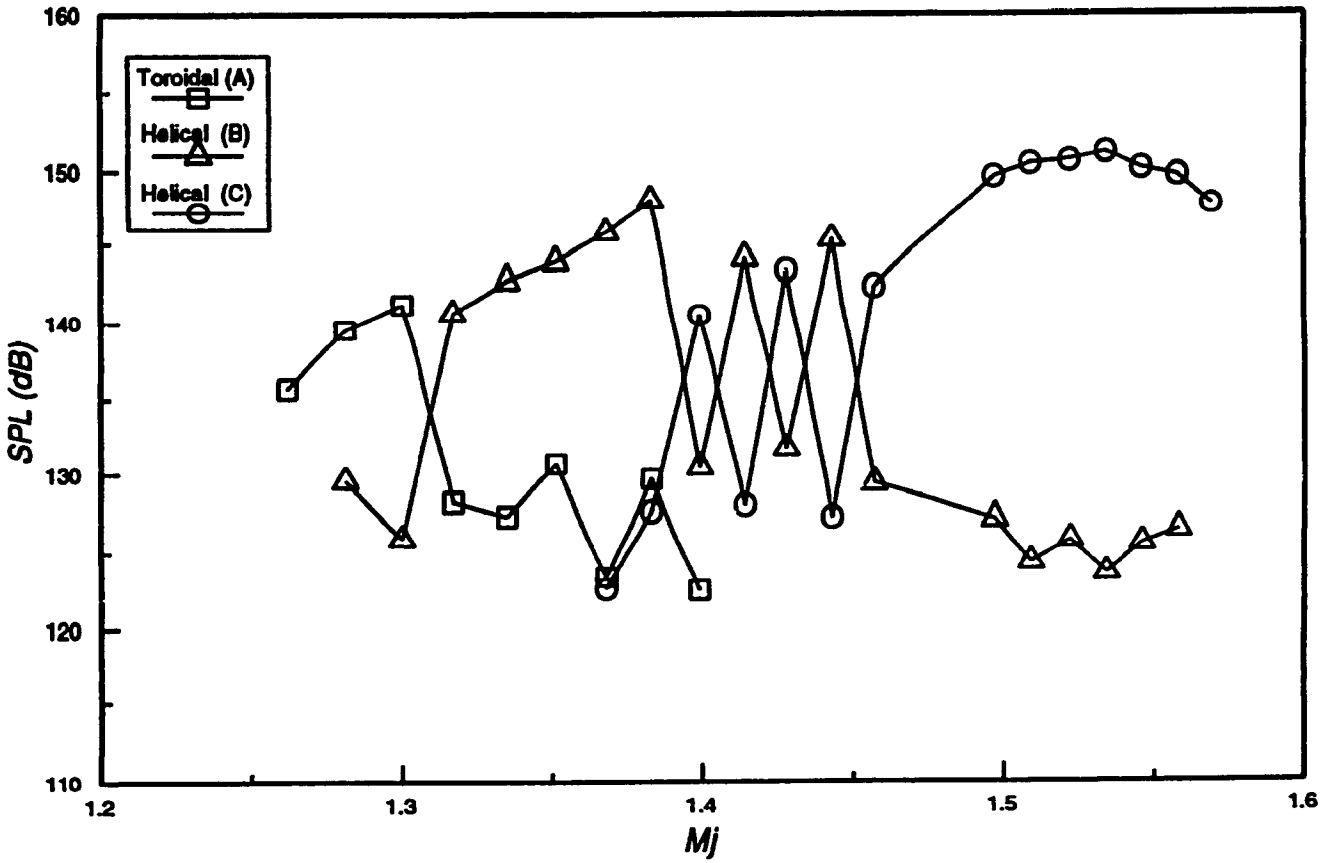

Figure 5.11 Sound pressure level for single jet

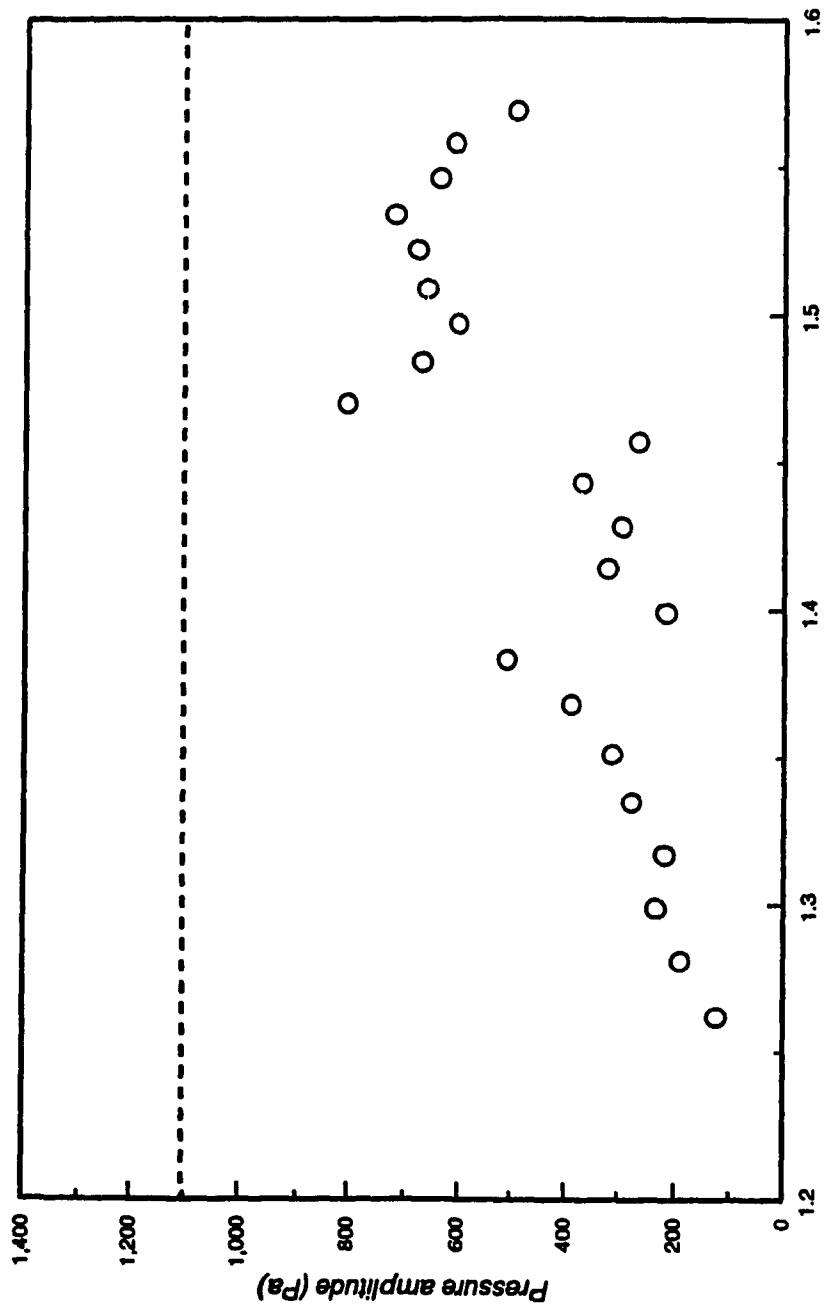

Figure 5.12 Pressure amplitude for single jet, ---- Sonic fatigue level

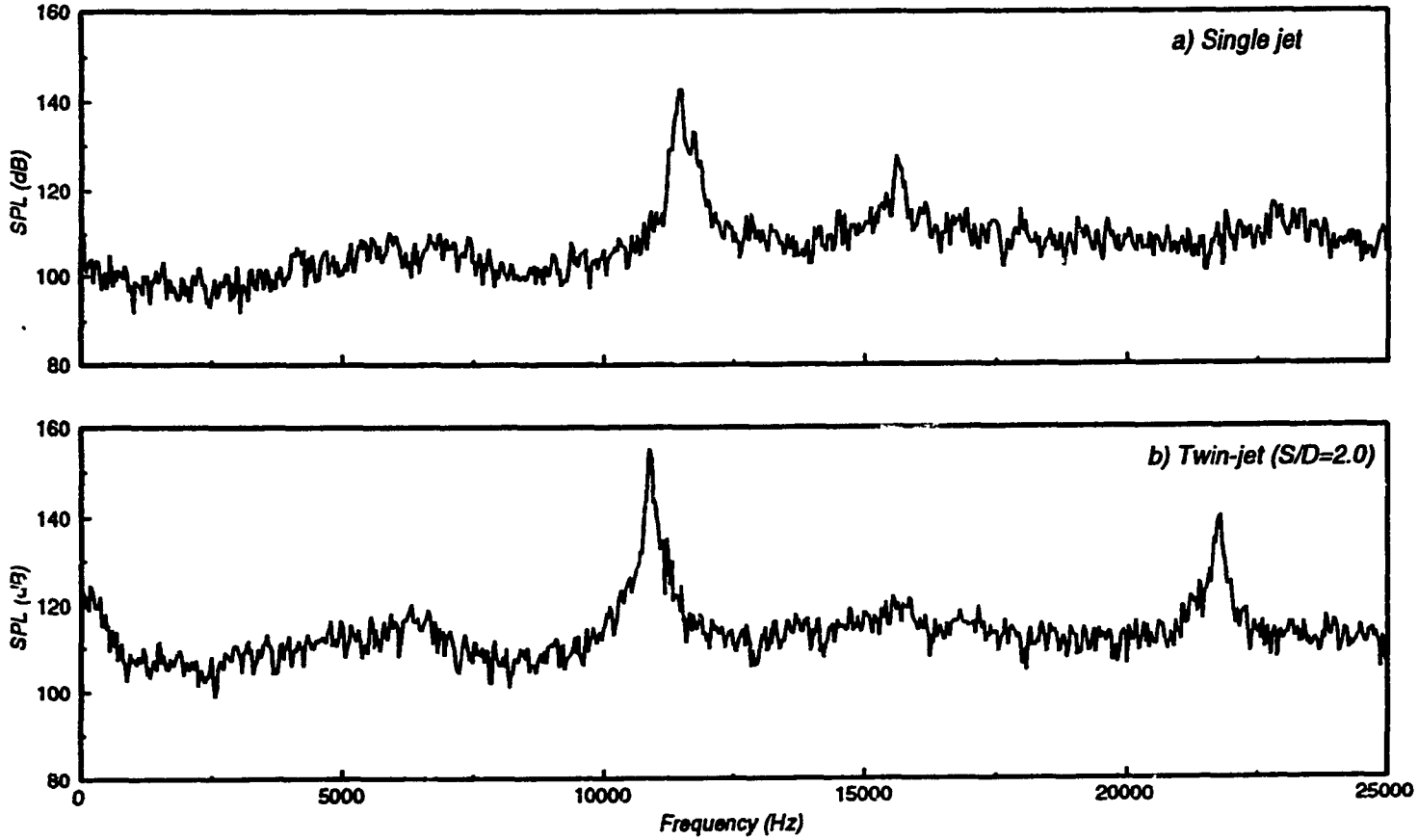

Figure 5.13 Effect of configuration on screech tone

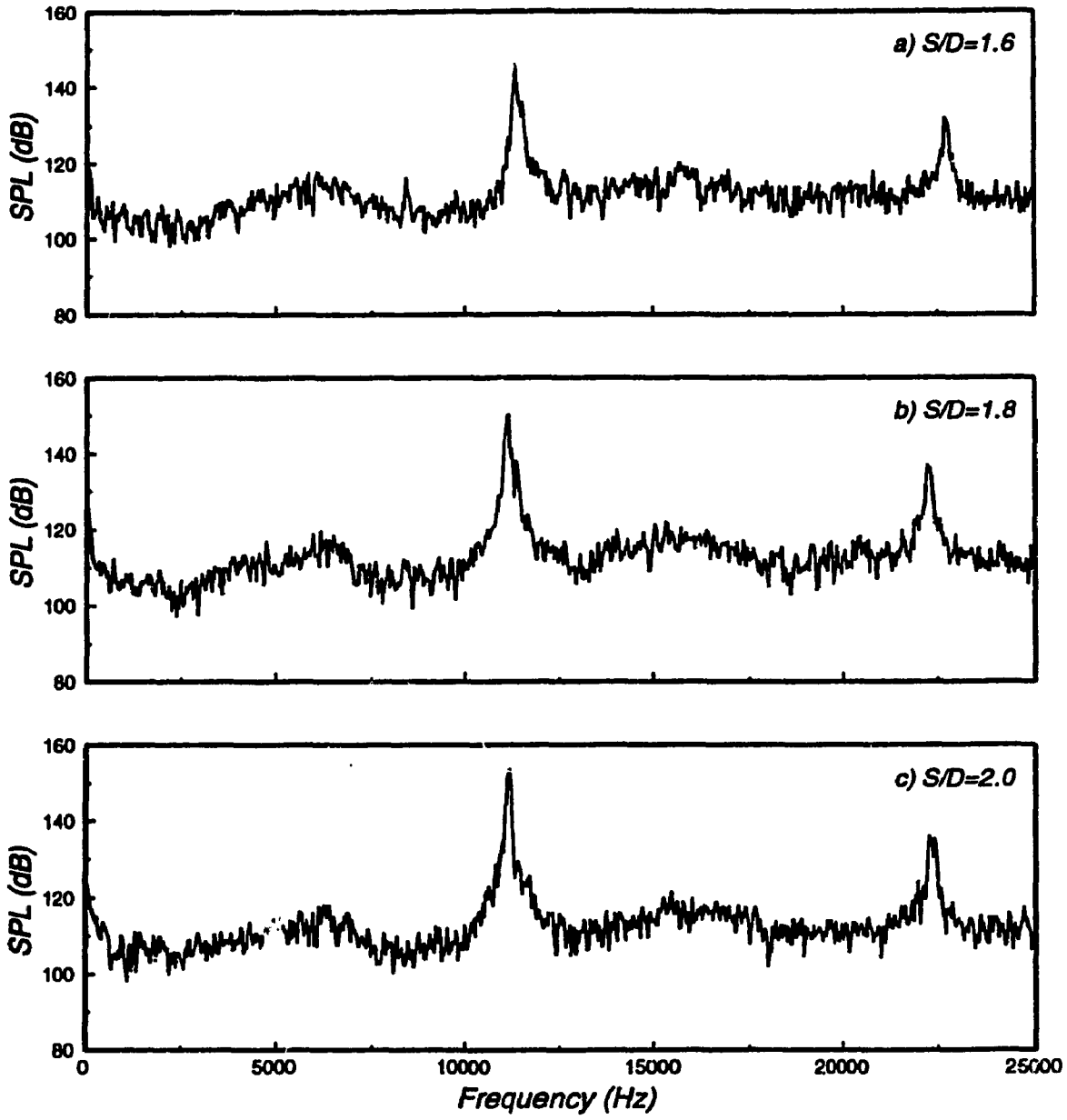

Figure 5.14 Effect of spacing on twin-jet screech tone, Mj =1.317

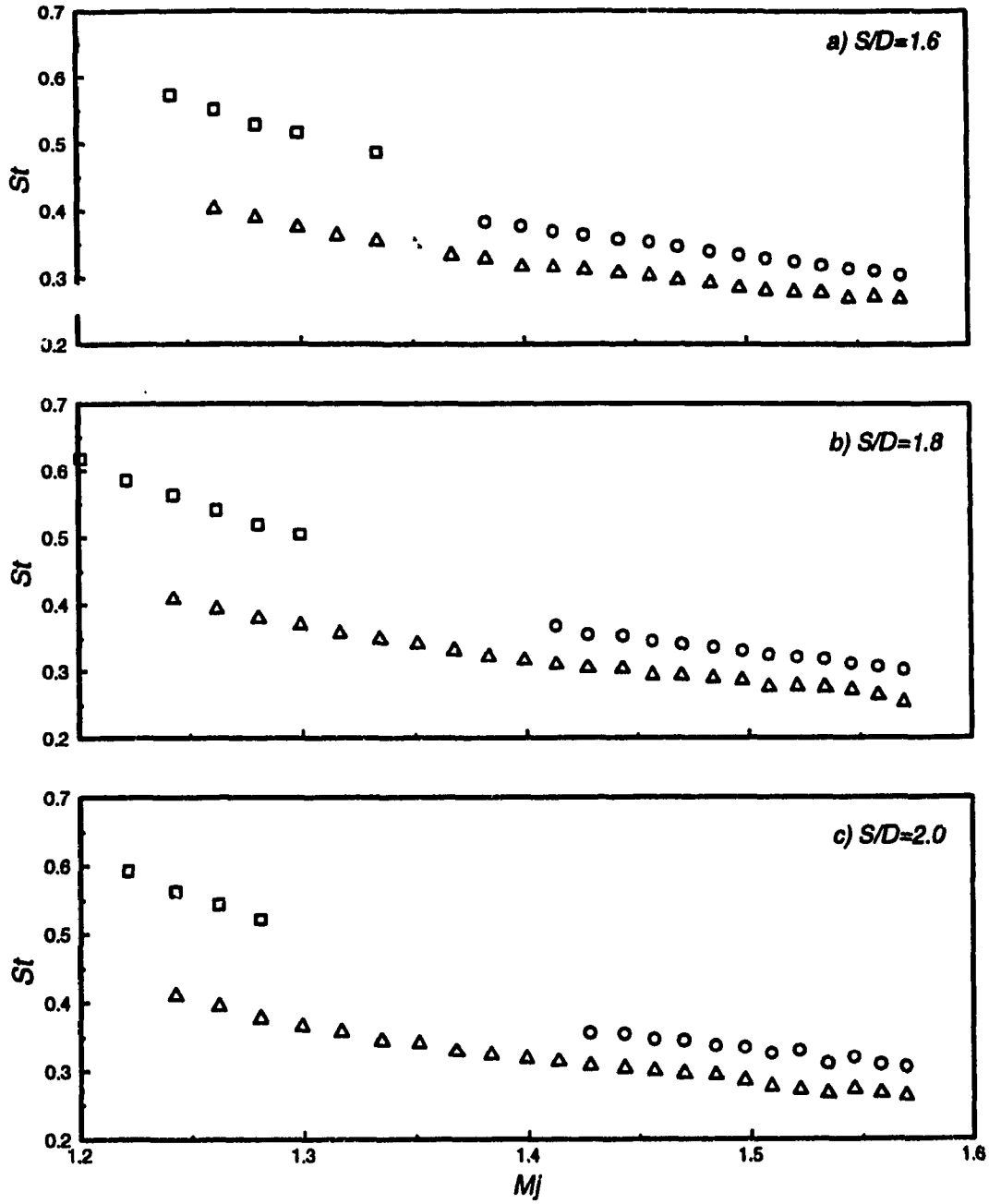

Figure 5.15 Strouhal numbers for twin jets,

□ Toroidal(A), △ Helical(B), ○Helical(C)

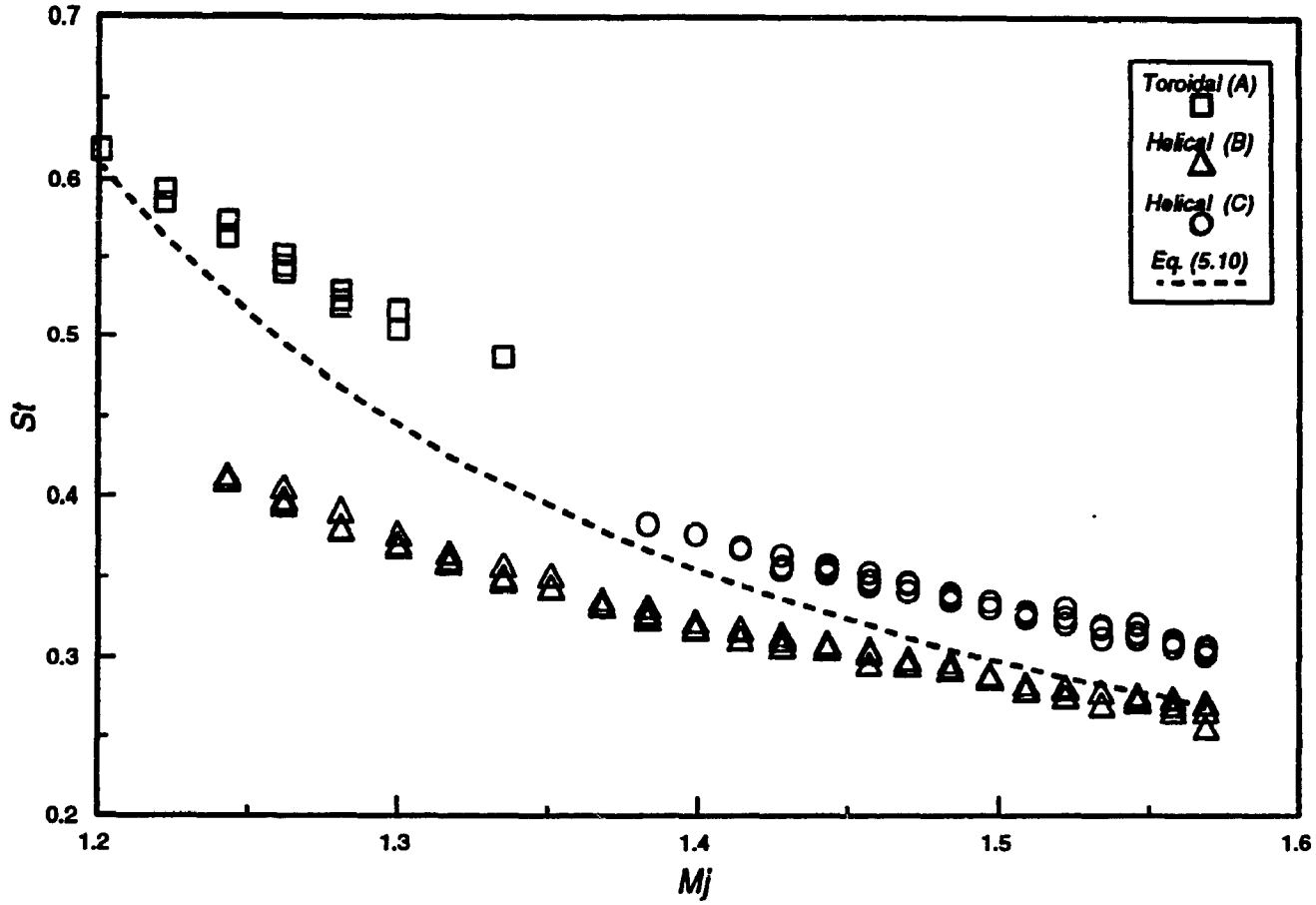

Figure 5.16 Composite Strouhal numbers for twin jets

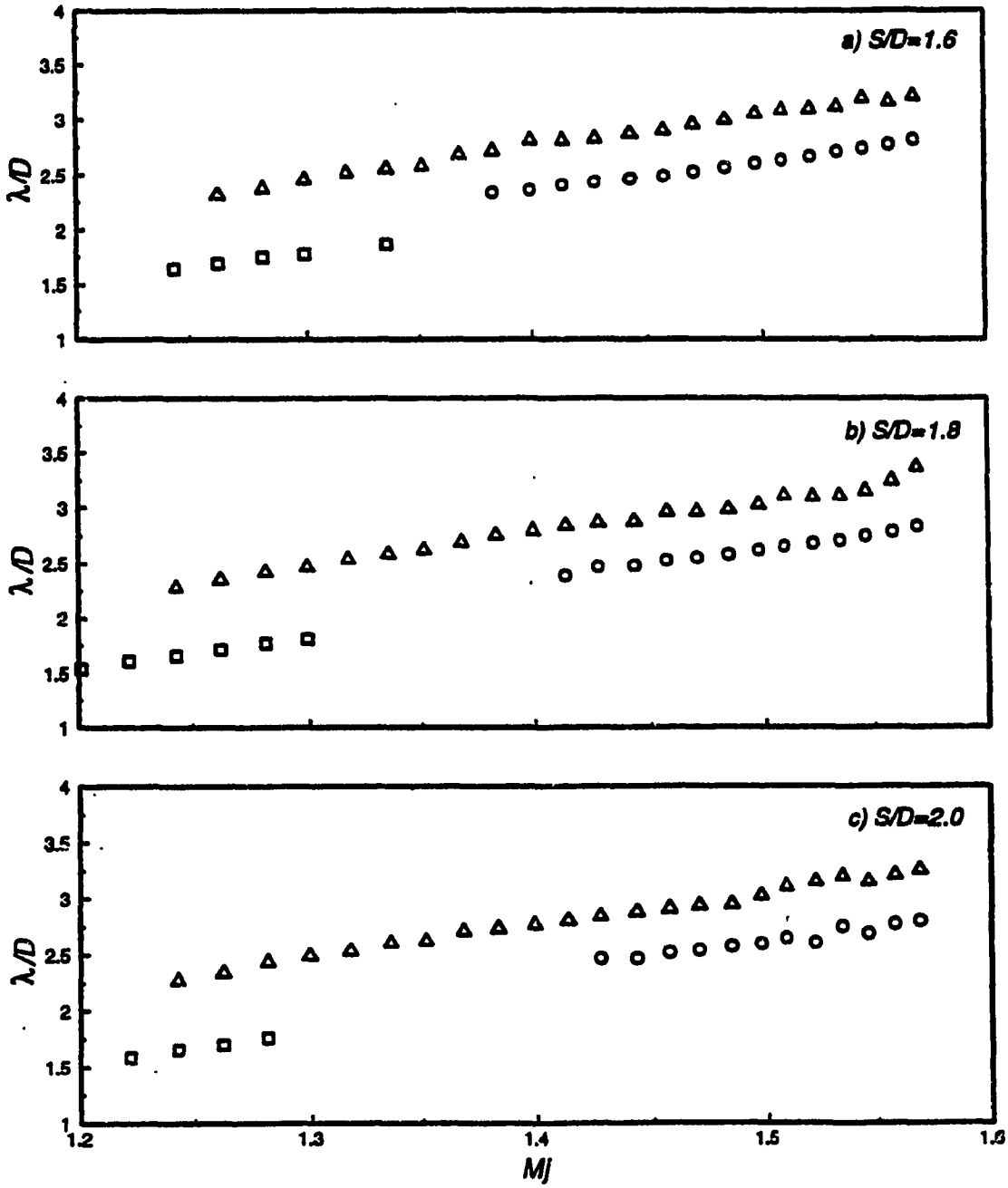

Figure 5.17 Screech tone wavelengths for twin jets,
□ Toroidal(A), △ Helical(B), ○ Helical(C)

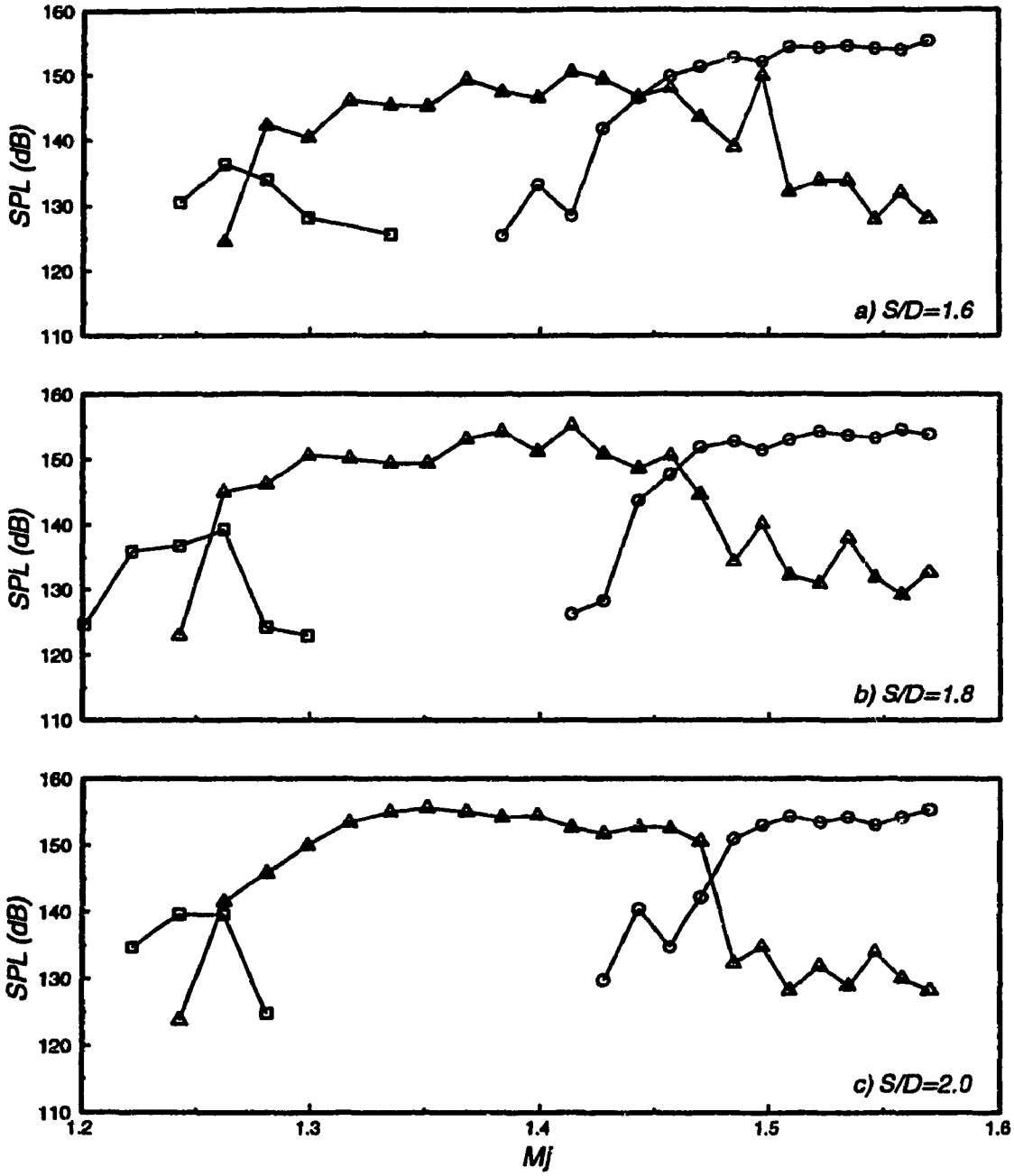

Figure 5.18 Sound pressure levels for twin jets,
□ Toroidal(A), △ Helical(B), ○ Helical(C)

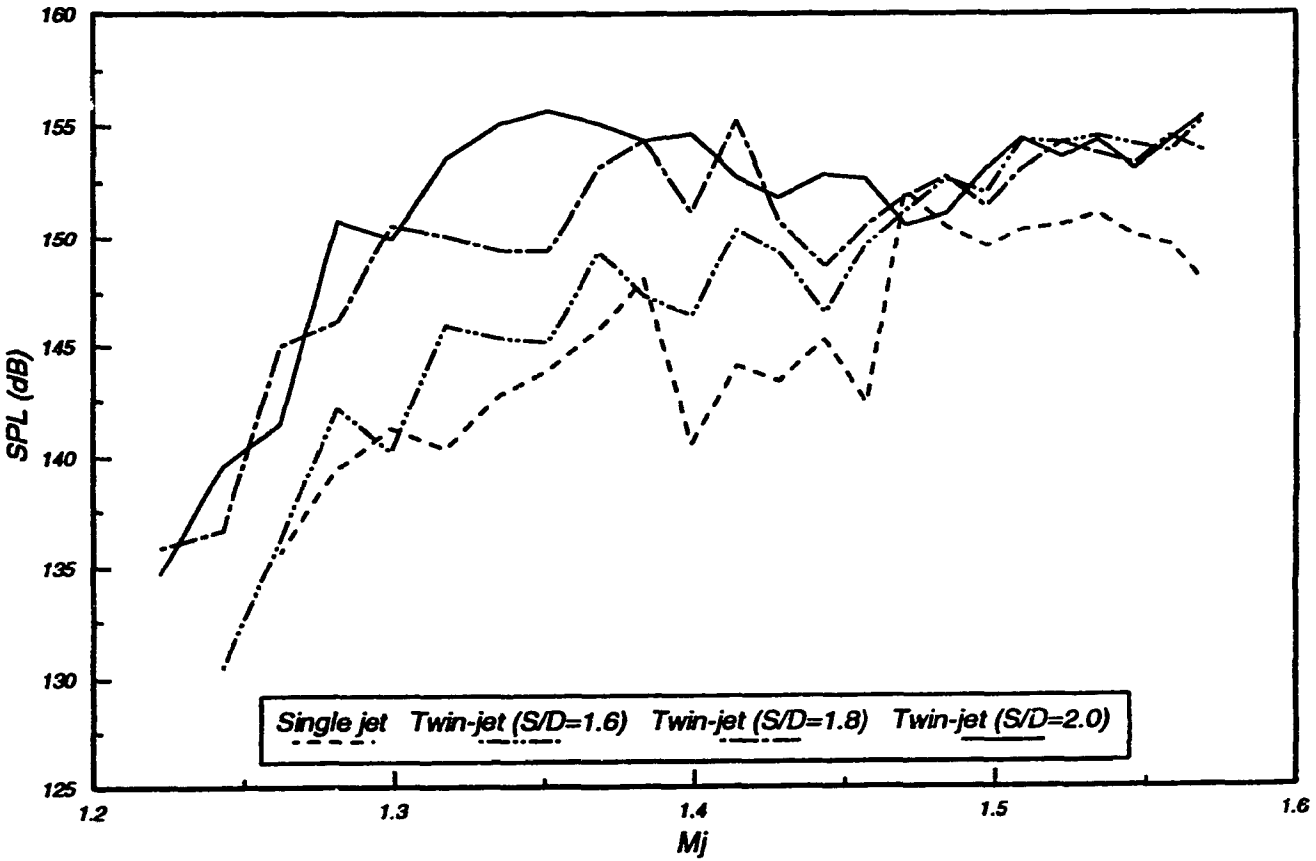

Figure 5.19 Maximum sound pressure levels for single and twin jets

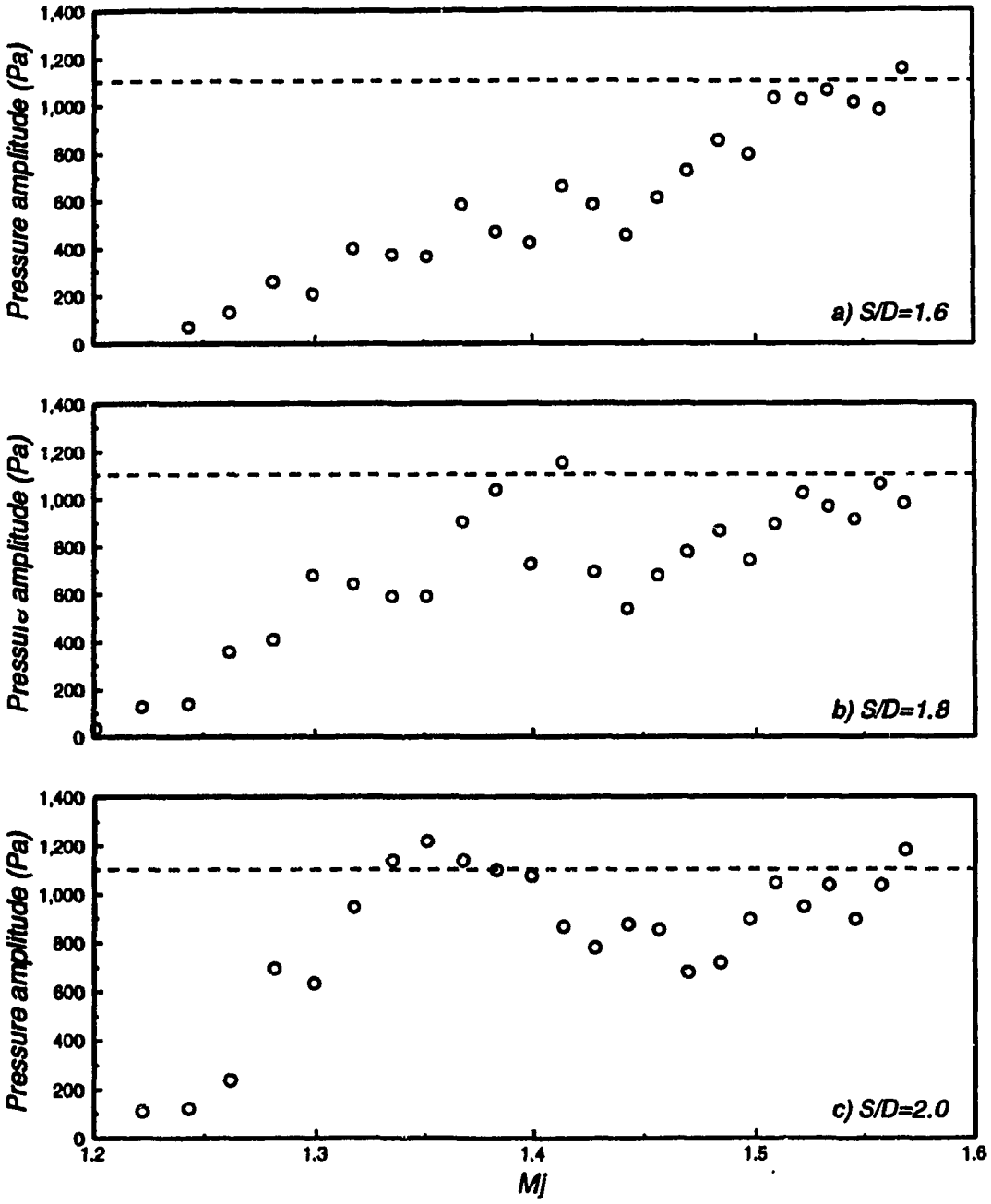

Figure 5.20 Pressure amplitudes for twin jets,

---- Sonic fatigue level

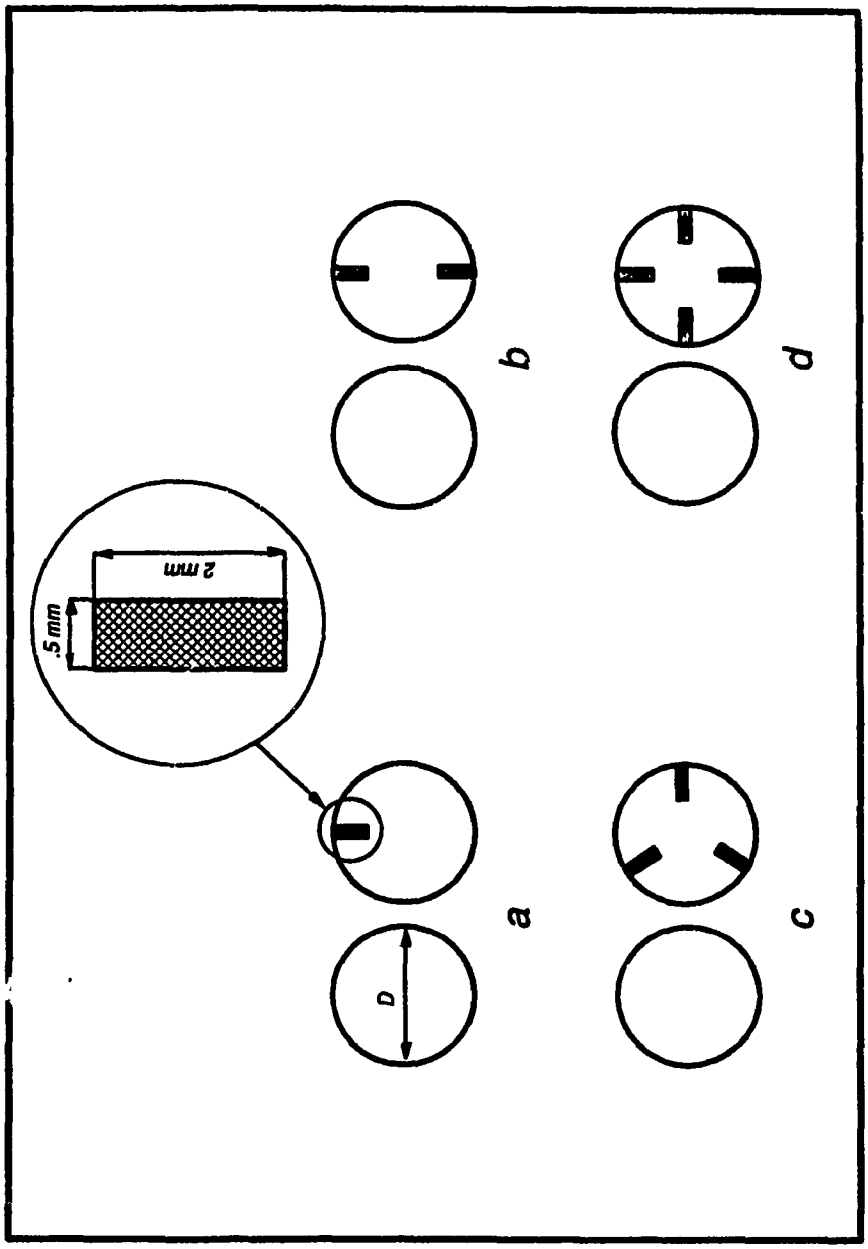

Figure 5.21 Sketch of tab along with installation on the model

a) 2 Tabs

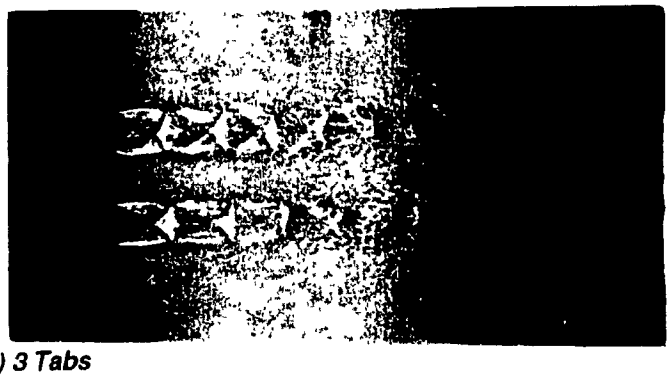

b) 3 Tabs

c) 4 Tabs

Figure 5.22 Effect of multi-tab on shock cell structures

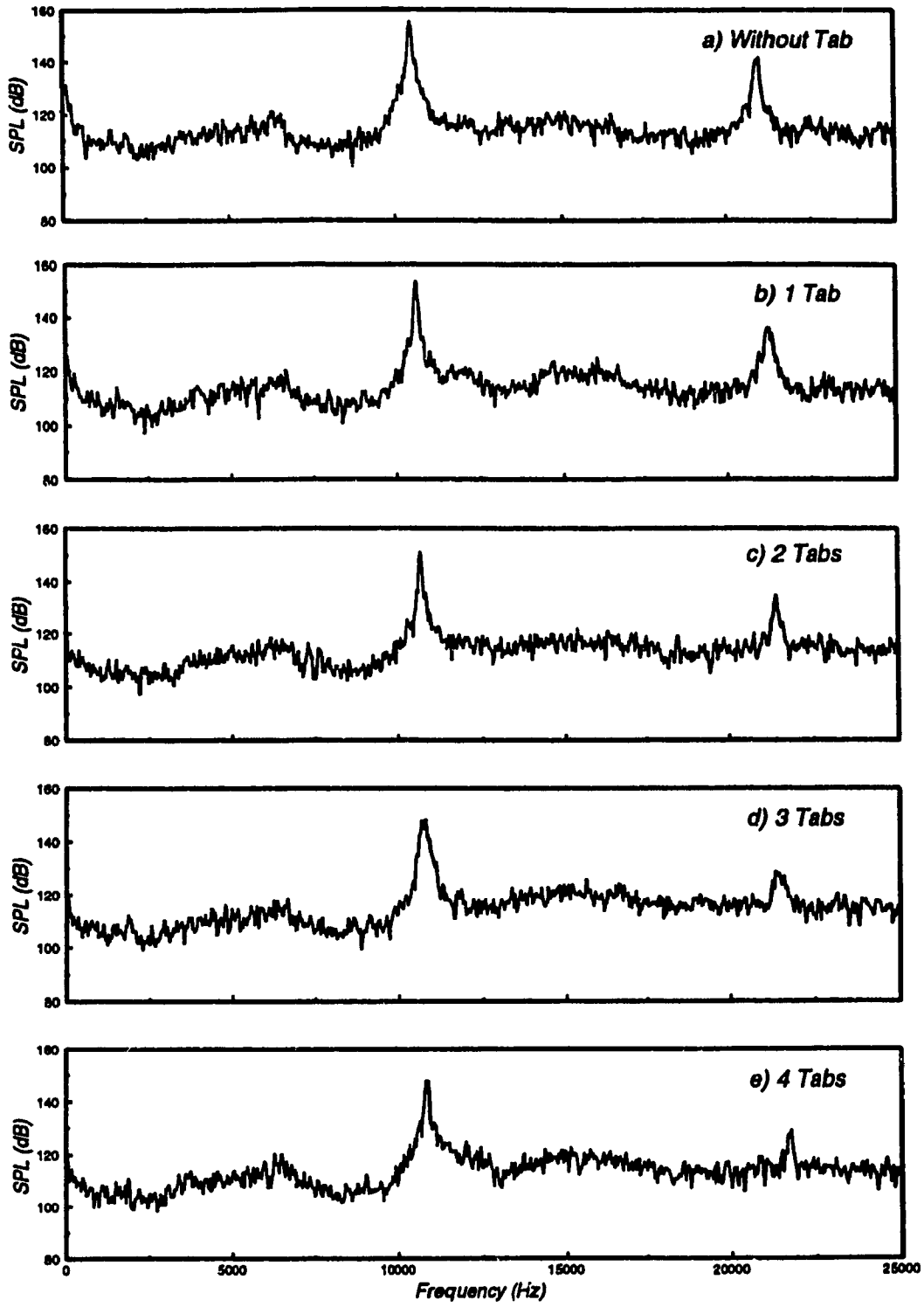

Figure 5.23 Effect of tab(s) on screech tone, Mj=1.368

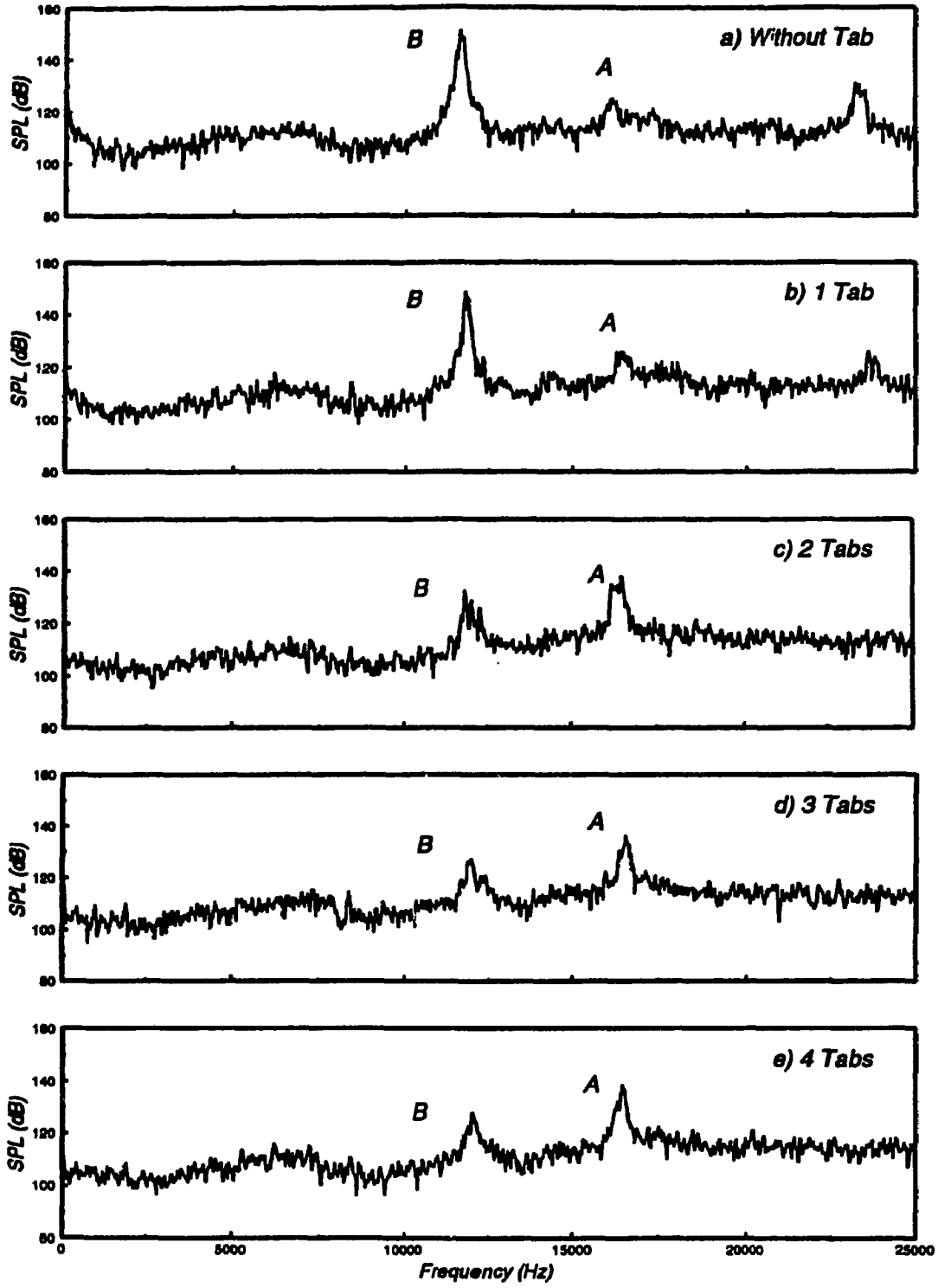

Figure 5.24 Effect of tab(s) on screech tone, Mj =1.281

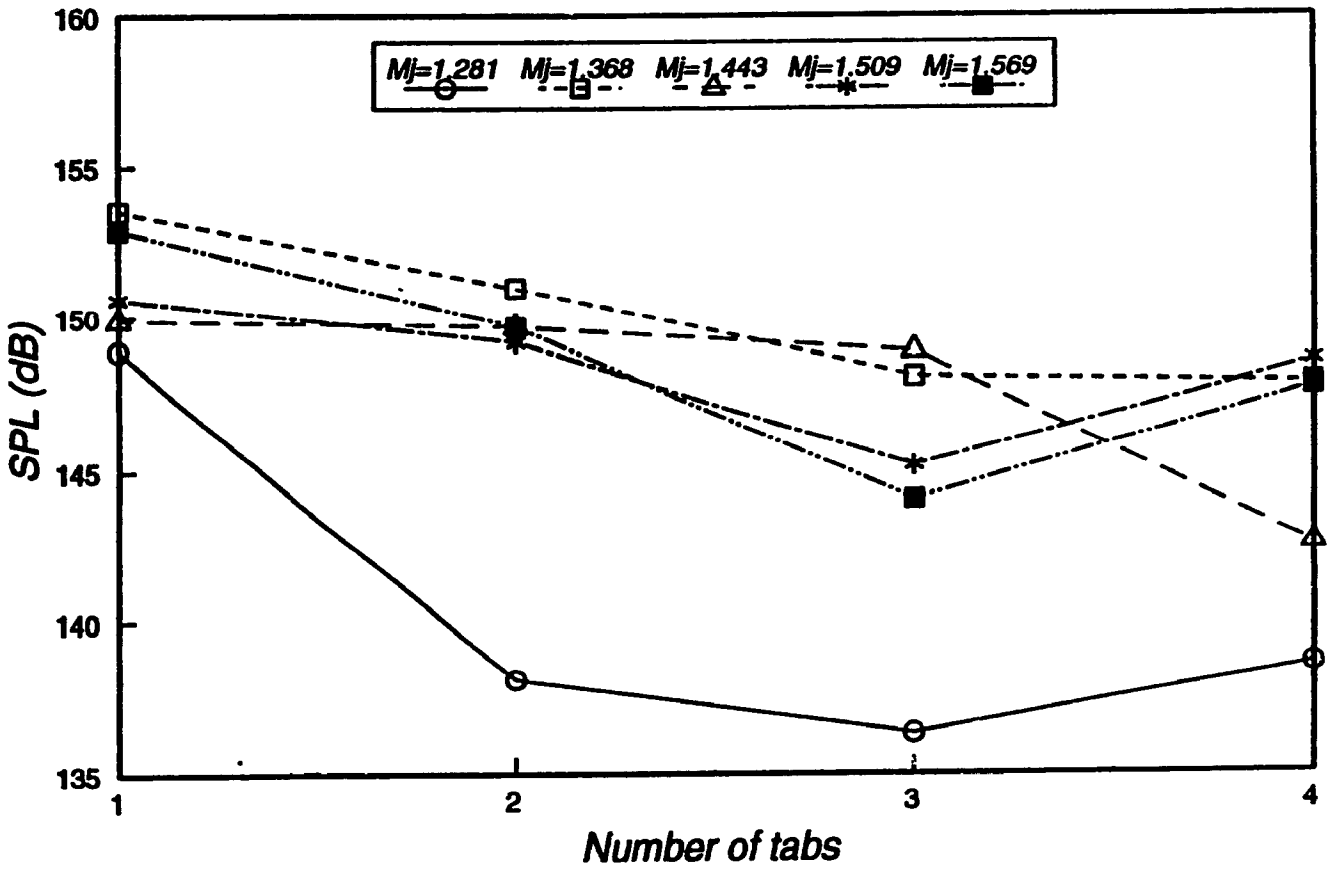

Figure 5.25 Effect of number of tab(s) on sound pressure level suppression

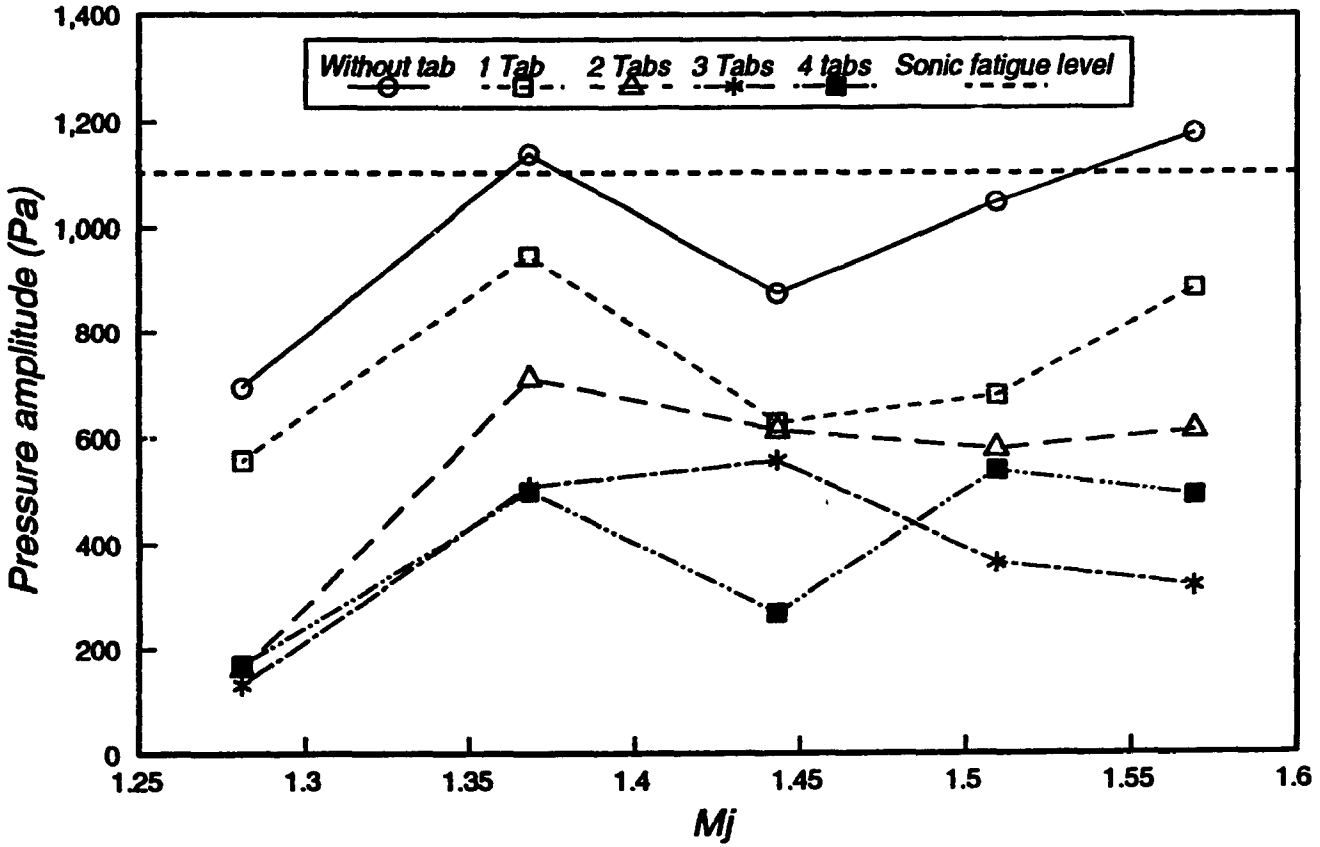

Figure 5.26 Pressure amplitude suppression with jet Mach number

REFERENCES

1. Tam. K. W., *On the Noise of a Nearly Ideally Expanded Supersonic Jet,* Journal of Fluid Mechanics, Vol. 51, Part 1, 1971, pp 69-87.

2. Powell. A., *On the Mechanism of Ckocked Jet Noise,* Proceedings of the Physical Society, London, Sec . B, Vol. 66, 1953, pp. 1039-1056.

3. Harper-Bourne, M. and Fisher, M. J., *The Noise from Shock Wave in Supersonic Jets,* AGARD-CP-131, 1973.

4. Shaw, L., *Twin-Jet Screech Suppression,* Journal of Aircraft, Vol. 27, No. 8, 1990 , pp. 708-715.

5. Norum, D. and Shearint. J. G ., *Dynamic Loads on Twin Jet Exhaust Nozzle Due to Shock Noise,* Journal of Aircraft, Vol. 23, No. 9, 1986, pp. 728-729.

6. Seiner, J. M., Manning, J. C. and Pontoon, M. K., *Dynamic Pressure Loads Associated With Twin Supersonic Plume Resonance,* AIAA Jorurnal , Vol. 26, No. 1988, pp. 954-960.

7. Berndt, D. E., *Dynamic Pressure Fluctuations In The Internozzle Region of a Twin Jet Nacelle,* Society of Automotive Engineers, Warrendale, PA, SAE-841540, 1984.

8. Wlezien, R. W., *Nozzle Geometry Effects on Supersonic Jet Interaction,* AIAA Paper 87-2694, 1987.

9. Seiner, J. M., Manning, J. C. and Ponton, M. K., *Model and Full Scale*

study of Twin Supersonic Plume Resonce, AIAA Paper 87-0244, 1987.

10. Laufer, J., Kaplan, R. E., Chu, W. T., *On the Generation of Jet Noise,* AGARD, No. 131.

11. J. E. A. John, *Gas Dynamics,* Allyn and Bacon, Inc. 1986.

12. Seiner, J. M., and Norum, T. D ., *Aerodynamic Aspects of Shock Containing Jet Plumes*, AIAA Paper 80-0965, 1980.

13. Seiner, J. M., Dash, S. M., Wolf, D. E., *Shock Noise Features Using the SCIPVIS Code,* AIAA Paper No.83-705, 1983.

14. Pao, P. S., Seiner, J. M., *Shock-Associated Noise in Supersonic Jets,* Vol. 21, No. 5, 1983, pp. 687-693.

15. Naumann, A., Hermanns, E., *On the Interaction Between a Shock Wave and a Vortex Field,* AGARD, No. 131.

16. Meadows, K.R., Kumar, A., and Hussaini, M.Y., *Computational Study on the Interaction Between a Vortex and Shock Wave,* AIAA Journal, Vol. 29, No. 2, 1991, pp. 174-179.

17. Tam, C. K. W., Tanna, H. K., *Shock Associated Noise of Supersonic Jets from Convergent-Divergent Nozzles,* Journal of Sound and Vibration, Vol. 81, No.3,1982, pp. 337-358.

18. Tam, C. T. W., Seiner, J. M., Yu, J. C., *Proposed Relationship Between Broadband Shock Associated Noise and Screech Tones,* Journal of Sound and Vibration, 110 (2), 1986, pp. 309-321.

19. Seiner, J. M., *Advances in High Speed Jet Aeroacoustics*, AIAA Paper 84-2275, 1984.

20. Roshford, T. J., Toms, H. L., *Recent Observations Including Temperature Dependence of Axisymmetric Jet Screech*, AIAA Journal, Vol. 13, No. 9, 1975, pp.1384-1386.

21. Drevet, P., Duponchel, J. P., Jacques, J. R., *Effect of Flight on Noise from a Convergent Nozzle as Observed on the Bertin Aerotrain*, AIAA Paper 76-557, 1976.

22. Bryce, W. D., Pinker, R. A., *The Noise from Unheated Supersonic Jets in Simulated Flight*, AIAA Paper 77-1327, 1977.

23. Sarohia, V., *Some Flight Simulation Experiments on Jet Noise from Supersonic Underexpanded Flows*, AIAA Journal, Vol. 16, No.7, 1978, pp. 710-716.

24. Norum, T. D., and Shearin, J. G., *Effects of Simulated Flight on the Structure and Noise of Underexpanded Jets*, NASA TP-2308, 1984.

25. Tam, C. K. W., Burton, D. E., *Sound Generated by Instability Waves of Supersonic Flows. Part 1 .Two Dimensional Mixing Layers and Part2.Axisymmetric Jets*, Journal of Fluid Mechanics, Vol.138, 1984, pp.249-295.

26. Morris, P. J., Tam, C. K. W., *Near and Far Field Noise from Large Scale Instabilities of Axisymmetric Jets*, AIAA Paper 77-1351, 1977.

27. McLaughlin, D. K., Morrison, G. L., Troutt, T. R., *Reynolds Number Dependence in Supersonic Jet Noise,* AIAA Journal, Vol. 15, 1977, pp.526-537.

28. Norum, T. D., *Screech suppression in Supersonic Jet,* AIAA Journal, Vol 21, No. 2, 1983, pp. 235-240.

29. Bradbury, L. J. S., and Khaden, A. H., *The Distortion of a Jet by Tabs,* Journal of Fluid Mechanics, Vol. 70, pt. 4, 1975, pp. 801-813.

30. Samimy, M., Zaman, K. B. M.,and Reeder, M. F., *Effect of Tabs on the Flow and Noise Field of an Axisymmetric Jet,* AIAA Journal, Vol 31, No. 4, 1993, pp 609-619.

31. Brüel & Kjær , *Product Data - Multichannel Analysis System,*.

32. A. G. Gaydon, and I. R. Hurle, *The Shock Tube in High-Temperature Chemical Physics,* Reinhold Publishing Corporation, 1963.

33. Davies, M. G. and Oldfield, D. E. S., *Tones from a Choked Axisymmetric Jet,* Acoustica. Vol. 12, 1962, pp. 257-277.

34. Powell, A. , Umeda, Y., and Ishii, R., *Observation of the Oscillation Modes of Chocked Circular Jets,* Journal of Acoust. Soc. Am. 1992 (5), November 1992, pp. 2823-2836.

35. Guinn, W. A., Balena, F. J., and Soovere, J., *Sonic Environment of Aircraft structure Immersed in a Supersonic and Jet Flow Stream,* NASA CR-144996, 1976.

APPENDIX A

BASIC OPTICAL PRINCIPLES

The optical method to be discussed here, which depend on the variation of density derivative throughout the flow field, is extremely important technique for the investigation of compressible flows [11]. The optical methods depend on the principle that the speed of light in a medium is dependent on the density of that medium. The index of refraction relates the speed of the light in vacuum c_o to the speed of light in a medium c .

$$n=\frac{c_o}{c} \tag{A.1}$$

For gases, the index of refraction is very close to 1, with

$$n=1+K_1\rho \tag{A.2}$$

where K_1 a positive constant.

As is well known, if light rays pass from one medium into another of different density, the rays are turned or refracted.

A series of light rays passing from air into water is shown in figure A.1. The plane wave front OA has been shown at the instant the light is incident on the surface. A short time later, the wave front reaches the position $O'A'$. Since the

velocity of light in water is less than in air, the distance OO' is less than AA', so the wave front turns, with

$$\frac{\sin i}{\sin r} = \frac{c_{air}}{c_{water}} = \frac{c_o/c_{water}}{c_o/c_{air}} = \frac{n_{water}}{n_{air}} \qquad \text{(A.3)}$$

Now suppose that, instead of a sudden change in n, the light passes through a region in which there exists a gradual change of index of refraction, as shown in figure A.2. In this case, there is a smooth turning of the light rays, with the angle through which the rays have been turned clearly dependent on the gradient of n which, in turn, is dependent on the density gradient in the y direction.

A two-dimensional flow in the z direction is shown in figure A.3, with a density gradient (perhaps caused by a shock) in the y direction.Light is to be passed through section AA in the x direction. It is assumed that the density decreases with y, so the velocity of light for ray 1 is greater than of ray 2. This causes a turning of the wave front and of the rays, as shown in figure A.4. Assume the density changes are relatively small so that the rays can be treated as straight lines. Let the velocity of light for ray 2 equal c, so the velocity of light for ray 1 will be $c+(dc/dy)\Delta y$. The angular deflection of the wave front and hence the angle through which the light rays are turned is given by

$$\Delta\alpha = \frac{\Delta t \frac{dc}{dy} \Delta y}{\Delta y} \tag{A.4}$$

where

$$\Delta t = \frac{L}{c} \tag{A.5}$$

Expanding this, we obtain

$$\Delta\alpha = \frac{dc}{dy}\frac{L}{c} \tag{A.6}$$

Substitution from Eqs. (A.1) and (A.2) yields

$$\Delta\alpha = -\frac{L}{n} K_1 \frac{d\rho}{dy} \tag{A.7}$$

For a three-dimensional flow, the angular deflection is dependent on the density gradient in both x and y directions. The important results is that the angular deflection of the light rays is dependent on the first derivative of density.

Having established the basic optical principles, the details of the schlieren system will be considered. The basic *schlieren* system is shown in figure A.5. Light from a source *ab* (for example, a filament) is collimated by lens l_1 , providing a parallel light rays from *a* and *b*, rays from each point passing parallel through the test section. After passing through the test section, the light rays are focused by

lens l_2 at $a'b'$, an inverted image of the light source. The light is then focused on the screen or photographic plate by lens l_3, providing an inverted image of the test section. Now a knife edge K is placed at $a'b'$. Clearly, if this knife edge is raised too far, it will obstruct all the light and the screen will be dark. Instead, let the knife edge obstruct approximately half the incident light. In this case, the image of the test section on the screen will be darker than before, but still uniformly illuminated; that is, the ray $rb'r'$ will reach the screen, but the ray $ra'r'$ will not, so the image of the point r will actually only half as bright as it would without the knife edge.

In the case, when there is a density gradient in the test section in the plane of r (same y coordinate as r), the rays from r will be deflected so that, for example, the ray $rb'r'$ will be turned downward, as shown, to the dashed line. Now this ray will be intercepted by the knife edge, so the image of r on the screen will be barker than the rest of the image of the test section. If the density gradient had the opposite sign, the rays from r would be bent upward, so some rays that had been obstructed by the knife edge would now pass over it and give a brighter image of r on the screen. In actual practice, it is found beneficial to use mirrors rather than lenses.

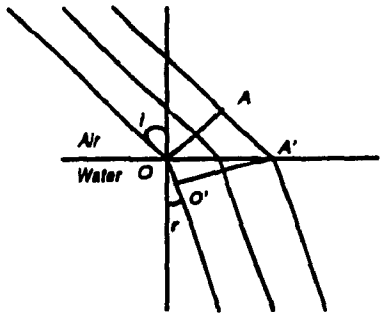

Figure A.1 Passing the light through a region with sudden change of n

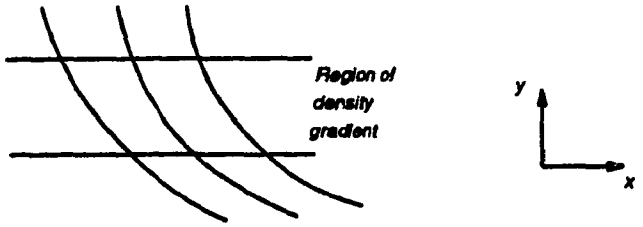

Figure A.2 Passing the light through a region with gradual change of n

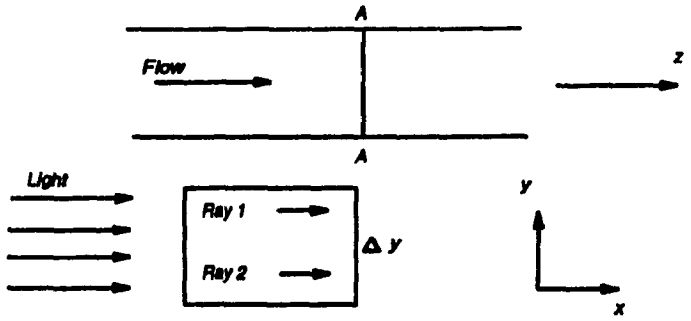

Figure A.3 Passing the light through a test section

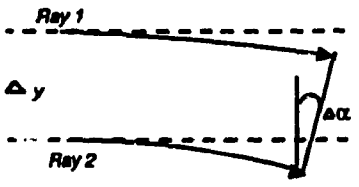

Figure A.4 Turning of the rays

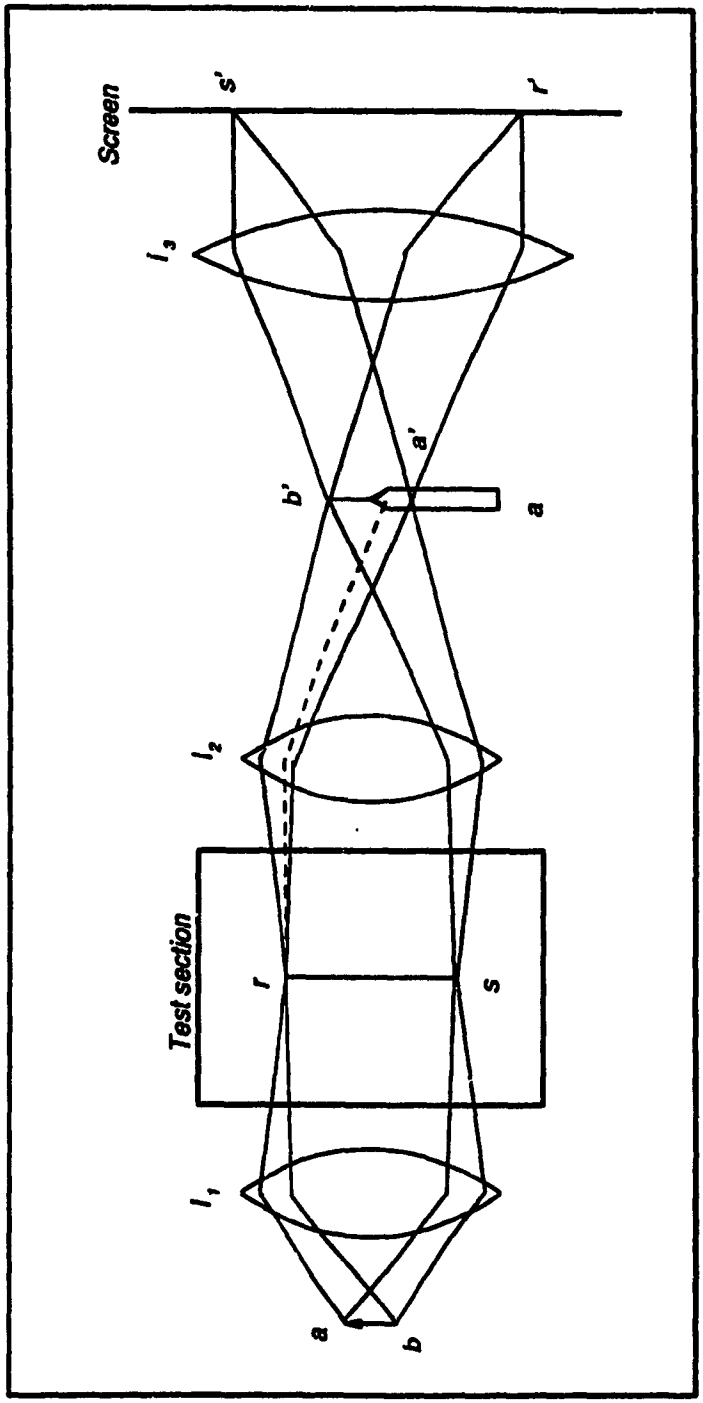

Figure A.5 Schlieren apparatus